AD-A064 386 VIRGINIA POLYTECHNIC INST AND STATE UNIV BLACKSBURG D--ETC F/G 19/5
A THREE DIMENSIONAL AUGMENTED SPHERICAL TRACKING FILTER FOR MAN--ETC(U)
1977 R L MOOSE, D H MCCABE N60921-78-C-A107

UNCLASSIFIED NL

| OF |
AD
A064386

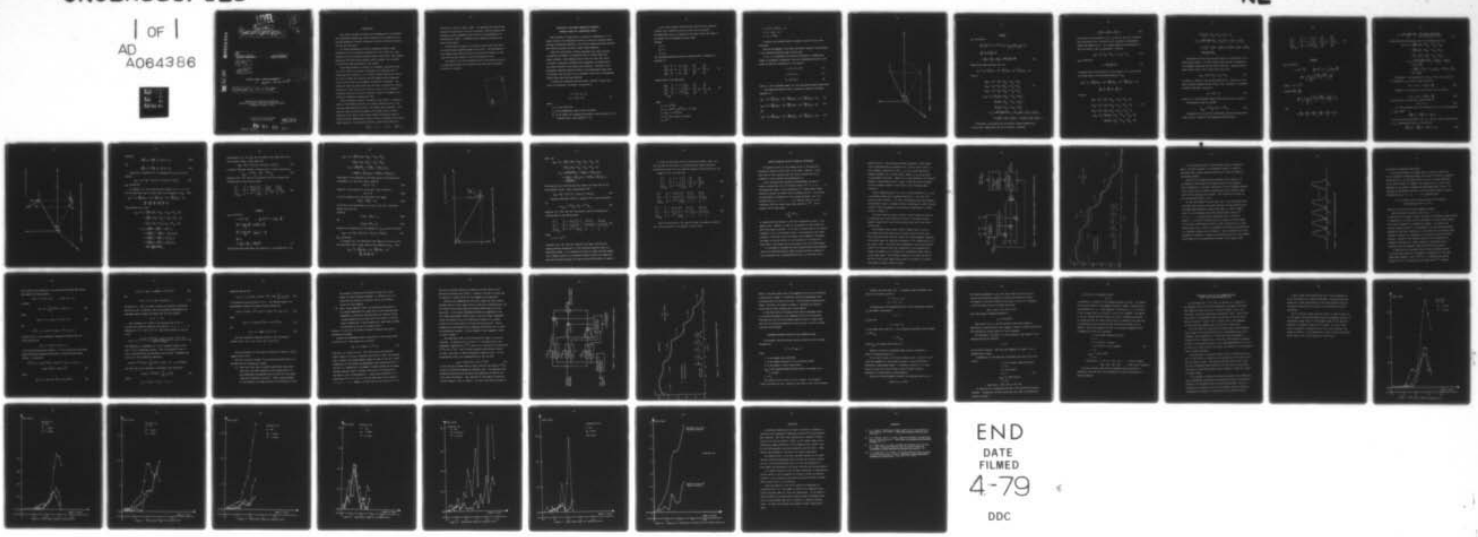

END
DATE
FILMED
4-79
DDC

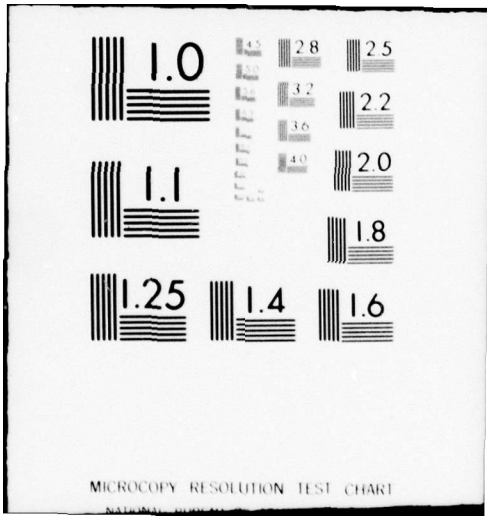
1.0
1.1
1.25
1.4
1.6
1.8
2.0
2.2
2.5
2.8
3.2
3.6
4.0
MICROCOPY RESOLUTION TEST CHART

LEVEL II

(2)

(9) FINAL REPORT,

(6) A THREE DIMENSIONAL AUGMENTED SPHERICAL TRACKING FILTER FOR MANEUVERING AIR TARGETS.

(10) Richard L. Moose
PRINCIPAL INVESTIGATOR

Denis H. McCabe
RESEARCH ASSOCIATE

(12) 49 p.

(11) 1977

CONTRACT NUMBER: ~~N60921-78-R-A073~~
or N60921-78-C-A107

(15) N60921-78-C-A107

Department of Electrical Engineering
Virginia Polytechnic Institute and State University
Blacksburg, Virginia 24061

Approved for Public Release
Distribution Unlimited

411062

INTRODUCTION

This report discusses the design and implementation of the adaptive three dimensional maneuvering target tracking filter in spherical coordinates, developed at Virginia Polytechnic Institute and State University over the past two years.

All filter performance statistics concerning intercept range, probability of kill, cumulative probability of kill, SIG3D, etc. were obtained from the statistical analysis program called GUSS. This program, supplied by the Naval Surface Weapons Center, Dahlgren, was installed on the VPI&SU computing system for this purpose.

Since GUSS performs its analysis in rectangular coordinates while the filter filters in spherical coordinates, two additional sets of subroutines were required to act as buffers between GUSS and the filter. The first of these sets converted the GUSS supplied three dimensional target position data from rectangular to spherical coordinates. The second set, which was much larger than the first, converted the filtered estimates of target position and velocity in each of the 3 spherical coordinate directions into their equivalent values in rectangular coordinates for subsequent processing by GUSS.

Unless otherwise specified, reference in this report to a predictor refers to the predictor used for fire control purposes and not to the one step ahead prediction process of the Kalman filter algorithm. This predictor takes the updated estimate of the target states at time k appearing at the output of each filter channel and predicts ahead an amount TP seconds (determined by GUSS) to yield an estimate of the future target position. This predicted position is then used by GUSS as an

"aim point" at which to shoot a shell. By comparing the actual target position TP seconds later with this "aim point", GUSS can compute miss distances in three dimensional space as well as the probability of destroying the target. A constant velocity spherical predictor was used in this report.

Over the past two years, two versions of this filter were used, the second being an improved design of the first. The performance of both designs using GUSS output will be analyzed with respect to each other and also with respect to the GIP rectangular filter.

The values of all filter parameters used in the various runs will be stipulated as also will be whether these values were arbitrarily arrived at or derived.

DERIVATION OF THE THREE DIMENSIONAL LINEARIZED SPHERICAL MODEL FOR A MANEUVERING TARGET

Exact modeling of target motion in spherical coordinates (r, e, β) usually involves the simultaneous solution of three very complex coupled nonlinear differential equations. The solution becomes even more difficult when forcing functions are used to model target maneuvers.

There are, nevertheless, several advantages which make filtering in spherical coordinates in conjunction with air target radar data, highly desirable. Chief amongst these is that the radar data itself is already in spherical coordinates and consequently the observations are linear functions of the target state variables. Therefore, if an approximate linearized spherical model for the maneuvering target could be obtained, then the need to use a nonlinear filter such as the Extended Kalman filter would have been obviated.

To derive the linearized spherical model, consider a target whose motion in rectangular coordinates is described by

$$\begin{aligned} \ddot{x} &= -\alpha\dot{x} + u_x + w_x' \\ \dot{w}_x' &= -aw_x' + w_x \end{aligned} \tag{1}$$

where

α is a drag coefficient

u_x is the deterministic input in the x direction

w_x' is the Singer [1] correlated acceleration process acting in the x direction with a time constant $\tau c = \frac{1}{a}$.

w_x is a white Gaussian random process acting in the x direction. A similar set of equations exists for the y and z directions. The significance of w_x' in relation to the final form of the filter to be derived, will be discussed in detail later.

Defining

$$x_1 = x$$

$$x_2 = \dot{x}$$

$$x_3 = w_x'$$

the following continuous time state variable model is obtained for equation (1)

$$\begin{bmatrix} \dot{x}_1 \\ \dot{x}_2 \\ \dot{x}_3 \end{bmatrix} = \begin{bmatrix} 0 & 1 & 0 \\ 0 & -\alpha & 1 \\ 0 & 0 & -a \end{bmatrix} \begin{bmatrix} x_1 \\ x_2 \\ x_3 \end{bmatrix} + \begin{bmatrix} 0 \\ 1 \\ 0 \end{bmatrix} u_x + \begin{bmatrix} 0 \\ 0 \\ 1 \end{bmatrix} w_x \qquad (2)$$

Discretizing (2) in time yields

$$\begin{bmatrix} x_1 \\ x_2 \\ x_3 \end{bmatrix}_{k+1} = \begin{bmatrix} 1 & A & B \\ 0 & E & F \\ 0 & 0 & e^{-at} \end{bmatrix} \begin{bmatrix} x_1 \\ x_2 \\ x_3 \end{bmatrix}_{k} + \begin{bmatrix} C \\ A \\ 0 \end{bmatrix} u_{x_k} + \begin{bmatrix} D \\ G \\ J \end{bmatrix} w_{x_k} \qquad (3)$$

where

$$A = (1 - e^{-\alpha T})/\alpha$$

$$B = [1 + (ae^{-\alpha T} - \alpha e^{-aT})/(\alpha - a)\ ]/(\alpha a)$$

$$C = (\alpha T - 1 + e^{-\alpha T})/\alpha^2$$

$$D = [T + (aA - \alpha J)/(\alpha - a)]/(\alpha a)$$

$$E = e^{-\alpha T}$$

$$F = (e^{-aT} - e^{-\alpha T})/(\alpha - a)$$

$$G = (J - A)/(\alpha - a)$$

$$J = (1 - e^{-aT})/a$$

A similar state variable model is assumed to exist for the y and z directions.

With the development of the above state model complete, the derivation of the linearized spherical model is given next.

If (x, y, z) represents the position coordinates of a maneuvering target in rectangular coordinates, then the corresponding position of the target in spherical coordinates is, from figure 1

$$r = (x^2 + y^2 + z^2)^{\frac{1}{2}} \tag{4}$$

$$e = \sin^{-1}(z/r) \tag{5}$$

$$\beta = \tan^{-1}(y/x) \tag{6}$$

where r, e and β represent range, elevation and bearing angles respectively.

The linearized spherical model is derived by using the following expansion [2]

$$r_{k+1} \simeq r_k + \frac{\partial r}{\partial x}\Big|_k (x_{k+1} - x_k) + \frac{\partial r}{\partial y}\Big|_k (y_{k+1} - y_k) + \frac{\partial r}{\partial z}\Big|_k (z_{k+1} - z_k) \tag{7a}$$

$$e_{k+1} \simeq e_k + \frac{\partial e}{\partial x}\Big|_k (x_{k+1} - x_k) + \frac{\partial e}{\partial y}\Big|_k (y_{k+1} - y_k) + \frac{\partial e}{\partial z}\Big|_k (z_{k+1} - z_k) \tag{7b}$$

and

$$\beta_{k+1} \simeq \beta_k + \frac{\partial \beta}{\partial x}\Big|_k (x_{k+1} - x_k) + \frac{\partial \beta}{\partial y}\Big|_k (y_{k+1} - y_k) + \frac{\partial \beta}{\partial z}\Big|_k (z_{k+1} - z_k) \tag{7c}$$

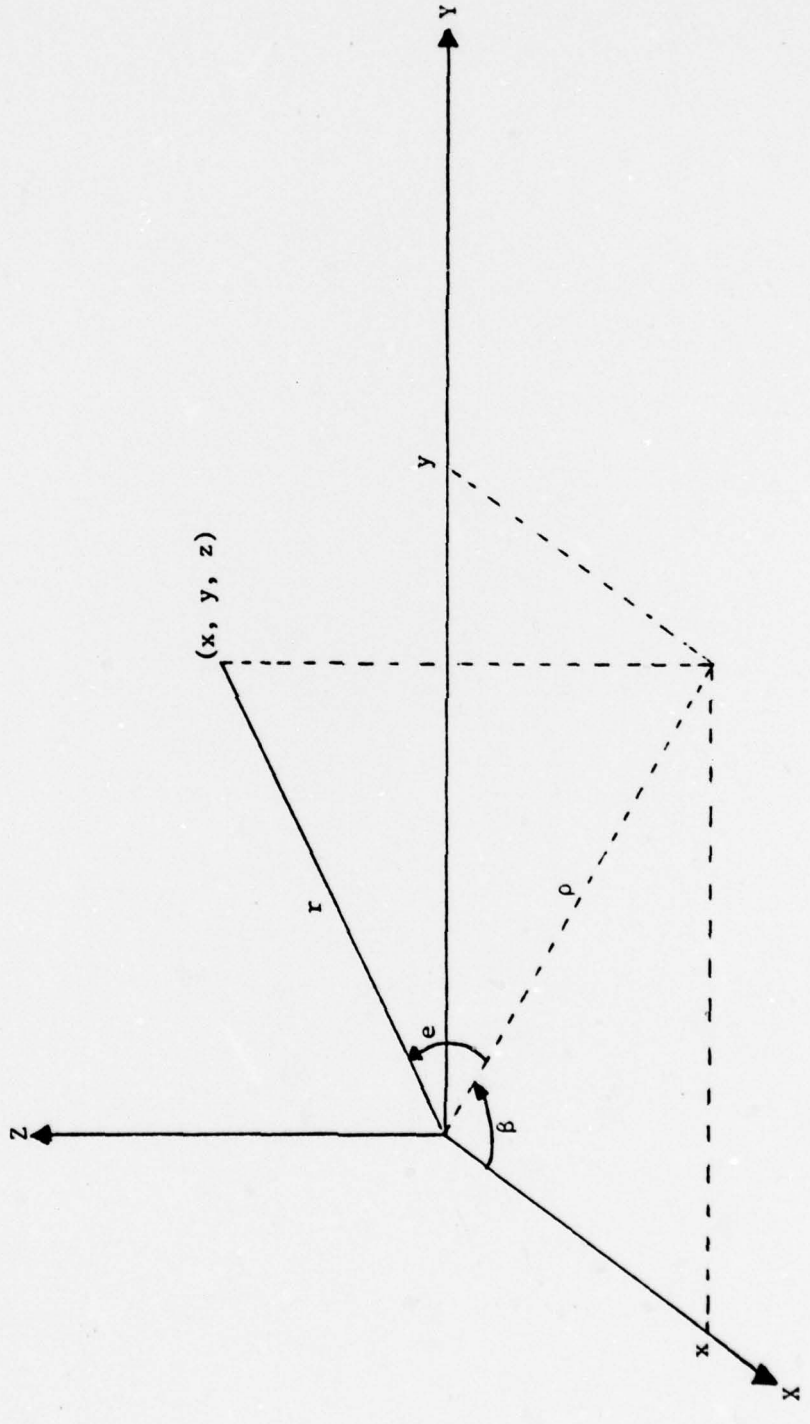

Figure 1. Target position in spherical coordinates.

r CHANNEL

r_{k+1} calculation:

$$\frac{\partial r}{\partial x} = \frac{1}{2}(x^2 + y^2 + z^2)^{-\frac{1}{2}} (2x) = \frac{x}{(x^2 + y^2 + z^2)^{\frac{1}{2}}} = \frac{x}{r}$$

$$\frac{\partial r}{\partial y} = \frac{y}{r} \text{ and } \frac{\partial r}{\partial z} = \frac{z}{r}$$

$$\dot{r} = \frac{\partial r}{\partial x}\dot{x} + \frac{\partial r}{\partial y}\dot{y} + \frac{\partial r}{\partial z}\dot{z} = \frac{(x\dot{x} + y\dot{y} + z\dot{z})}{r} \tag{8}$$

Substituting these relations into 7(a)

$$r_{k+1} = r_k + \frac{x}{r}\Big|_k (x_{k+1} - x_k) + \frac{y}{r}\Big|_k (y_{k+1} - y_k) + \frac{z}{r}\Big|_k (z_{k+1} - z_k)$$

From (3)

$$\begin{aligned}
(x_{k+1} - x_k) &= A\dot{x}_k + Bw_{x_k}' + Cu_{x_k} + Dw_{x_k} \\
(y_{k+1} - y_k) &= A\dot{y}_k + Bw_{y_k}' + Cu_{y_k} + Dw_{y_k} \qquad (9) \\
(z_{k+1} - z_k) &= A\dot{z}_k + Bw_{z_k}' + Cu_{z_k} + Dw_{z_k}
\end{aligned}$$

$$\begin{aligned}
\therefore r_{k+1} &= r_k + \frac{x}{r}\Big|_k [A\dot{x}_k + Bw_{x_k}' + Cu_{x_k} + Dw_{x_k}] + \\
&\quad \frac{y}{r}\Big|_k [A\dot{y}_k + Bw_{y_k}' + Cu_{y_k} + Dw_{y_k}] + \\
&\quad \frac{z}{r}\Big|_k [A\dot{z}_k + Bw_{z_k}' + Cu_{z_k} + Dw_{z_k}] \\
&= r_k + A\left[\frac{x\dot{x} + y\dot{y} + z\dot{z}}{r}\right]\Big|_k + B\left[w_x'\left(\frac{x}{r}\right) + w_y'\left(\frac{y}{r}\right) + w_z'\left(\frac{z}{r}\right)\right]\Big|_k \\
&\quad + C\left[u_x\left(\frac{x}{r}\right) + u_y\left(\frac{y}{r}\right) + u_z\left(\frac{z}{r}\right)\right]\Big|_k + D\left[w_x\left(\frac{x}{r}\right) + w_y\left(\frac{y}{r}\right) + w_z\left(\frac{z}{r}\right)\right]\Big|_k
\end{aligned}$$

From Figure 1, $\frac{x}{r}$, $\frac{y}{r}$ and $\frac{z}{r}$ are the direction cosines between the X, Y and Z axes, respectively, and the r direction. Therefore

$$w_x'(\frac{x}{r}) + w_y'(\frac{y}{r}) + w_z'(\frac{z}{r}) \equiv w_r' \tag{10}$$

is the sum of the projections of w_x', w_y' and w_z' onto the r direction. This sum acting in the r direction can be replaced by an equivalent single term denoted by w_r'. In a similar manner the coefficients of C and D are called u_r and w_r respectively. Using (8)

$$r_{k+1} = r_k + A\dot{r}_k + Bw_r'_k + C\,u_{r_k} + D\,w_{r_k} \tag{11}$$

$\dot{r}_{k+1}$ calculation:

$$\dot{r} = \frac{x\dot{x} + y\dot{y} + z\dot{z}}{r} \tag{8}$$

In equation (8) the derivatives of $\dot{r}$ with respect to $\dot{x}$, $\dot{y}$ and $\dot{z}$ yield the linear terms in the following expansion of $\dot{r}_{k+1}$

$$\dot{r}_{k+1} \approx \dot{r}_k + \frac{\partial \dot{r}}{\partial \dot{x}}\Big|_k(\dot{x}_{k+1} - \dot{x}_k) + \frac{\partial \dot{r}}{\partial \dot{y}}\Big|_k(\dot{y}_{k+1} - \dot{y}_k) + \frac{\partial \dot{r}}{\partial \dot{z}}\Big|_k(\dot{z}_{k+1} - \dot{z}_k)$$

$$\frac{\partial \dot{r}}{\partial \dot{x}} = \frac{x}{r}\,,\quad \frac{\partial \dot{r}}{\partial \dot{y}} = \frac{y}{r}\,,\quad \frac{\partial \dot{r}}{\partial \dot{z}} = \frac{z}{r}$$

From (3)

$$\begin{aligned}
(\dot{x}_{k+1} - \dot{x}_k) &= E\dot{x}_k + Fw_x'_k + Au_{x_k} + Gw_{x_k} - \dot{x}_k \\
(\dot{y}_{k+1} - \dot{y}_k) &= E\dot{y}_k + Fw_y'_k + Au_{y_k} + Gw_{y_k} - \dot{y}_k \\
(\dot{z}_{k+1} - \dot{z}_k) &= E\dot{z}_k + Fw_z'_k + Au_{z_k} + Gw_{z_k} - \dot{z}_k \\
\therefore \dot{r}_{k+1} &= \dot{r}_k + \frac{x}{r}\Big|_k[E\dot{x}_k + Fw_x'_k + Au_{x_k} + Gw_{x_k} - \dot{x}_k] \\
&\quad + \frac{y}{r}\Big|_k[E\dot{y}_k + Fw_y'_k + Au_{y_k} + Gw_{y_k} - \dot{y}_k]
\end{aligned} \tag{12}$$

$$+ \frac{z}{r}\Big|_k [E\dot{z}_k + Fw_{z_k}' + Au_{z_k} + Gw_{z_k} - \dot{z}_k]$$

$$= \dot{r}_k + E[\frac{x\dot{x} + y\dot{y} + z\dot{z}}{r}]_k + F[w_x'(\frac{x}{r}) + w_y'(\frac{y}{r}) + w_z'(\frac{z}{r})]_k$$

$$+ A[u_x(\frac{x}{r}) + u_y(\frac{y}{r}) + u_z(\frac{z}{r})]_k + G[w_x(\frac{x}{r}) + w_y(\frac{y}{r}) + w_z(\frac{z}{r})]_k$$

$$- [\frac{x\dot{x} + y\dot{y} + z\dot{z}}{r}]_k$$

From equation (8) the first and last terms on the right side of the above equality cancel. The other terms involve the sum of projections of rectangular quantities onto the radial direction. Treating these as single terms acting in the r direction we end up with

$$\dot{r}_{k+1} = E\dot{r}_k + Fw_{r_k}' + Au_{r_k} + Gw_{r_k} \tag{13}$$

It remains to obtain a state variable model for w_r'. Since w_r' is a zero mean correlated Gaussian process acting in the r direction, a convenient continuous time model is given by

$$\dot{w}_r' = -aw_r' + w_r \tag{14}$$

where w_r is a white Gaussian random process acting in the r direction.

Discretized in time (14) becomes

$$w_{r_{k+1}}' = e^{-aT}w_{r_k}' + \frac{1}{a}(1 - e^{-aT})w_{r_k} \tag{15}$$

Equations (11), (13) and (15) collectively form the following state model for the r channel of the linearized spherical model:

$$\begin{bmatrix} r \\ \dot{r} \\ w'_r \end{bmatrix}_{k+1} = \begin{bmatrix} 1 & A & B \\ 0 & E & F \\ 0 & 0 & e^{-aT} \end{bmatrix} \begin{bmatrix} r \\ \dot{r} \\ w'_r \end{bmatrix}_k + \begin{bmatrix} C \\ A \\ 0 \end{bmatrix} u_{r_k} + \begin{bmatrix} D \\ G \\ J \end{bmatrix} w_{r_k} \qquad (16)$$

e CHANNEL

e_{k+1} calculation:

$$e = \sin^{-1}\left\{\frac{z}{r}\right\} \qquad \frac{d}{dx}\left[\sin^{-1} u\right] = \frac{1}{(1 - u^2)^{\frac{1}{2}}} \frac{du}{dx}$$

$$\frac{\partial e}{\partial x} = \frac{1}{\left(1 - \frac{z^2}{r^2}\right)^{\frac{1}{2}}} \left\{ \frac{r(0) - z\left(\frac{x}{r}\right)}{r^2} \right\} = \frac{-xz}{\rho r^2}$$

where $\rho = (x^2 + y^2)^{\frac{1}{2}}$

Similarly $\frac{\partial e}{\partial y} = \frac{-yz}{\rho r^2}$

$$\frac{\partial e}{\partial z} = \frac{1}{\left(1 - \frac{z^2}{r^2}\right)^{\frac{1}{2}}} \left\{ \frac{r(1) - z\left(\frac{z}{r}\right)}{r^2} \right\} = \frac{r}{\rho} \left\{ \frac{\rho^2}{r^3} \right\} = \frac{\rho}{r^2}$$

and

$$\dot{e} = \frac{\partial e}{\partial x} \dot{x} + \frac{\partial e}{\partial y} \dot{y} + \frac{\partial e}{\partial z} \dot{z} = \frac{-xz}{\rho r^2} \dot{x} - \frac{yz}{\rho r^2} \dot{y} + \frac{\rho}{r^2} \dot{z}$$

$$\therefore \dot{e} = \frac{\rho^2\dot{z} - (x\dot{x} + y\dot{y})z}{\rho r^2} = \frac{(x^2 + y^2)\dot{z} - (x\dot{x} + y\dot{y})z}{(x^2 + y^2)^{\frac{1}{2}}(x^2 + y^2 + z^2)} \tag{17}$$

Substituting these derivatives into 7(b) and making use of (9)

$$\begin{aligned} e_{k+1} = e_k &+ \left(\frac{-xz}{\rho r^2}\right)\Big|_k [A\dot{x}_k + Bw_{x_k}' + Cu_{x_k} + Dw_{x_k}] \\ &+ \left(\frac{-yz}{\rho r^2}\right)\Big|_k [A\dot{y}_k + Bw_{y_k}' + Cu_{y_k} + Dw_{y_k}] \\ &+ \left(\frac{\rho}{r^2}\right)\Big|_k [A\dot{z}_k + Bw_{z_k}' + Cu_{z_k} + Dw_{z_k}] \\ = e_k &+ A\left[\frac{-(x\dot{x} + y\dot{y})z + \rho^2\dot{z}}{\rho r^2}\right]_k + B\left[\frac{-xz}{\rho r} w_x' + \frac{-yz}{\rho r} w_y'\right. \\ &\left. + \frac{\rho}{r} w_z'\right]_k \left(\frac{1}{r}\right)_k \\ &+ C\left[\frac{-xz}{\rho r} u_x - \frac{yz}{\rho r} u_y + \frac{\rho}{r} u_z\right]_k \left(\frac{1}{r}\right)_k + D\left[\frac{-xz}{\rho r} w_x - \frac{yz}{\rho r} w_y\right. \\ &\left. + \frac{\rho}{r} w_z\right]_k \left(\frac{1}{r}\right)_k \end{aligned}$$

From figure 2, the projection of the unit vector in the direction of increasing e, i_e, ontothe X axis is given by

$$-\sin e \cos \beta = -\left(\frac{z}{r}\right)\left(\frac{x}{\rho}\right) = \frac{-xz}{\rho r} \tag{18a}$$

Similarly, the projection of i_e onto the Y axis is given by

$$-\sin e \sin \beta = -\left(\frac{z}{r}\right)\left(\frac{y}{\rho}\right) = \frac{-yz}{\rho r} \tag{18b}$$

The projection of i_e onto the Z axis is given by

$$\cos e = \rho/r \tag{18c}$$

In view of equation (18), the coefficient of B in the above expansion of e_{k+1}, namely

$$\left(\frac{-xz}{\rho r}\right) w_x' + \left(\frac{-yz}{\rho r}\right) w_y' + \left(\frac{\rho}{r}\right) w_z'$$

is the sum of the projections of w_x', w_y', and w_z' acting in the direction of i_e; denoting this sum as w_e' we have that

$$\left(\frac{-xz}{\rho r}\right) w_x' + \left(\frac{-yz}{\rho r}\right) w_y' + \left(\frac{\rho}{r}\right) w_z' \equiv w_e' \tag{19a}$$

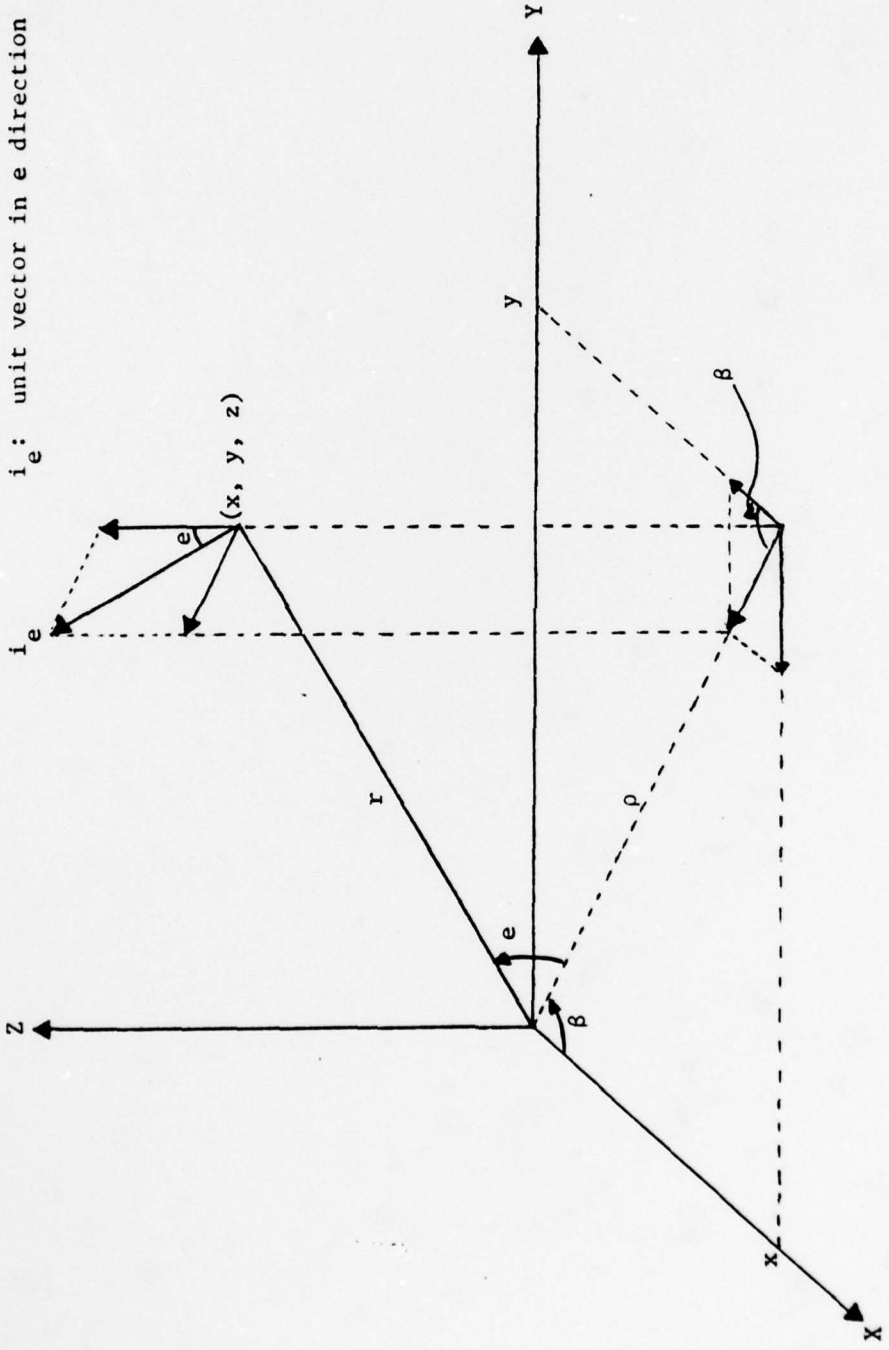

Figure 2: Direction cosines between i_e and the X, Y, and Z axes.

Similarly

$$\left(\frac{-xz}{\rho r}\right) u_x + \left(\frac{-yz}{\rho r}\right) u_y + \left(\frac{\rho}{r}\right) u_z = u_e \tag{19b}$$

and

$$\left(\frac{-xz}{\rho r}\right) w_x + \left(\frac{-yz}{\rho r}\right) w_y + \left(\frac{\rho}{r}\right) w_z = w_e \tag{19c}$$

Taking note of equation (17), the expansion for e_{k+1} can now be written

$$e_{k+1} \simeq e_k + A\dot{e}_k + B(w_e'/r)_k + C(u_e/r)_k + D(w_e/r)_k \tag{20}$$

$\dot{e}_{k+1}$ calculation:

In equation (17), the derivatives with respect to $\dot{x}$, $\dot{y}$, and $\dot{z}$ are the only ones which lead to linear terms in the expansion of $\dot{e}_{k+1}$. Thus,

$$\dot{e}_{k+1} \simeq \dot{e}_k + \frac{\partial \dot{e}}{\partial \dot{x}}\Big|_k (\dot{x}_{k+1} - \dot{x}_k) + \frac{\partial \dot{e}}{\partial \dot{y}}\Big|_k (\dot{y}_{k+1} - \dot{y}_k) + \frac{\partial \dot{e}}{\partial \dot{z}}\Big|_k (\dot{z}_{k+1} - \dot{z}_k)$$

$$\frac{\partial \dot{e}}{\partial \dot{x}} = \frac{-xz}{\rho r^2}, \quad \frac{\partial \dot{e}}{\partial \dot{y}} = \frac{-yz}{\rho r^2}, \quad \frac{\partial \dot{e}}{\partial \dot{z}} = \frac{\rho}{r^2}$$

Using equation (12) we get

$$\begin{aligned}
\dot{e}_{k+1} = \dot{e}_k &+ \left(\frac{-xz}{\rho r^2}\right)\Big|_k [E\dot{x}_k + Fw_{x_k}' + Au_{x_k} + Gw_{x_k} - \dot{x}_k] \\
&+ \left(\frac{-yz}{\rho r^2}\right)\Big|_k [E\dot{y}_k + Fw_{y_k}' + Au_{y_k} + Gw_{y_k} - \dot{y}_k] \\
&+ \left(\frac{\rho}{r^2}\right)\Big|_k [E\dot{z}_k + Fw_{z_k}' + Au_{z_k} + Gw_{z_k} - \dot{z}_k] \\
= \dot{e}_k &+ E\left[\left(\frac{-xz}{\rho r^2}\right)\dot{x} + \left(\frac{-yz}{\rho r^2}\right)\dot{y} + \left(\frac{\rho}{r^2}\right)\dot{z}\right]_k \\
&+ F\left[\left(\frac{-xz}{\rho r}\right)w_x' + \left(\frac{-yz}{\rho r}\right)w_y' + \left(\frac{\rho}{r}\right)w_z'\right]_k / r_k \\
&+ A\left[\left(\frac{-xz}{\rho r}\right)u_x + \left(\frac{-yz}{\rho r}\right)u_y + \left(\frac{\rho}{r}\right)u_z\right]_k / r_k \\
&+ G\left[\left(\frac{-xz}{\rho r}\right)w_x + \left(\frac{-yz}{\rho r}\right)w_y + \left(\frac{\rho}{r}\right)w_z\right]_k / r_k \\
&- \left[\frac{\rho^2\dot{z} - (x\dot{x} + y\dot{y})z}{\rho r^2}\right]_k
\end{aligned}$$

From equation (17), the first and last terms on the right side of the above equality cancel. Hence using (19)

$$\dot{e}_{k+1} = E\dot{e}_k + F(w_e'/r)_k + A(u_e/r)_k + G(w_e/r)_k \tag{21}$$

A discrete time model similar to equation (15) is used to describe w_e':

$$w_{e_{k+1}}' = e^{-at} w_{e_k}' + \frac{1}{a}(1 - e^{-at}) w_{e_k} \tag{22}$$

Equations (20), (21), and (22) collectively form the following state variable model in the elevation plane:

$$\begin{bmatrix} e \\ \dot{e} \\ w_e' \end{bmatrix}_{k+1} = \begin{bmatrix} 1 & A & (B/r_k) \\ 0 & E & (F/r_k) \\ 0 & 0 & e^{-at} \end{bmatrix} \begin{bmatrix} e \\ \dot{e} \\ w_e' \end{bmatrix}_k + \begin{bmatrix} C/r_k \\ A/r_k \\ 0 \end{bmatrix} u_{e_k} + \begin{bmatrix} D/r_k \\ G/r_k \\ J \end{bmatrix} w_{e_k} \tag{23}$$

β CHANNEL

β_{k+1} calculation:

$$\beta = \tan^{-1}\left(\frac{y}{x}\right) \qquad \frac{d}{dx}\left[\tan^{-1} u\right] = \frac{1}{1 + u^2}\,\frac{du}{dx}$$

$$\frac{\partial \beta}{\partial x} = \frac{1}{1 + \frac{y^2}{x^2}}\left(\frac{-y}{x^2}\right) = \frac{-y}{x^2 + y^2} = \frac{-y}{\rho^2}$$

$$\frac{\partial \beta}{\partial y} = \frac{1}{1 + \frac{y^2}{x^2}}\left(\frac{1}{x}\right) = \frac{x}{x^2 + y^2} = \frac{x}{\rho^2}$$

$$\frac{\partial \beta}{\partial z} = 0$$

$$\dot{\beta} = \frac{\partial \beta}{\partial x}\dot{x} + \frac{\partial \beta}{\partial y}\dot{y} = \frac{-y\dot{x} + x\dot{y}}{\rho^2} \tag{24}$$

Substituting these derivatives into equation 7(c) and making use of (9)

$$\beta_{k+1} = \beta_k + \left(\frac{-y}{\rho^2}\right)\Big|_k \left[A\dot{x}_k + Bw_{x_k}' + Cu_{x_k} + Dw_{x_k}\right]$$

$$+ \left(\frac{x}{\rho^2}\right)\Big|_k \left[A\dot{y}_k + Bw_{y_k}' + Cu_{y_k} + Dw_{y_k}\right]$$

$$= \beta_k + A\left[\frac{y\dot{x} + x\dot{y}}{\rho^2}\right]_k + B\left[\left(\frac{-y}{\rho}\right)w_x' + \left(\frac{x}{\rho}\right)w_y'\right]_k/\rho_k$$

$$+ C\left[\left(\frac{-y}{\rho}\right)u_x + \left(\frac{x}{\rho}\right)u_y\right]_k/\rho_k + D\left[\left(\frac{-y}{\rho}\right)w_x + \left(\frac{x}{\rho}\right)w_y\right]_k/\rho_k$$

From figure 3, the projection of the unit vector in the direction of increasing β, i_β, onto the X axis is given by

$$-\sin\beta = -\frac{y}{\rho} \tag{25a}$$

Similarly, the projection of i_β onto the Y axis is given by

$$\cos\beta = \frac{x}{\rho} \tag{25b}$$

In view of equation (25), the coefficient of B, namely

$$\left(-\frac{y}{\rho}\right)w_x' + \left(\frac{x}{\rho}\right)w_y' \equiv w_\beta' \tag{26a}$$

is the sum of the projections of w_x' and w_y' onto the i_β direction. Denote this sum by w_β'.

Similarly

$$\left(-\frac{y}{\rho}\right)u_x + \left(\frac{x}{\rho}\right)u_y \equiv u_\beta \tag{26b}$$

and

$$\left(-\frac{y}{\rho}\right)w_x + \left(\frac{x}{\rho}\right)w_y \equiv w_\beta \tag{26c}$$

Taking note of equation (24), the expansion of β_{k+1} can now be written

$$\beta_{k+1} = \beta_k + A\dot{\beta}_k + B(w_\beta'/\rho)_k + C(u_\beta/\rho)_k + D(w_\beta/\rho)_k \tag{27}$$

$\dot{\beta}_{k+1}$ calculation:

In equation (24), the derivatives with respect to $\dot{x}$ and $\dot{y}$ are the only ones which lead to linear terms in the expansion of $\dot{\beta}_{k+1}$. Thus,

$$\dot{\beta}_{k+1} = \dot{\beta}_k + \frac{\partial\dot{\beta}}{\partial\dot{x}}\Big|_k(\dot{x}_{k+1} - \dot{x}_k) + \frac{\partial\dot{\beta}}{\partial\dot{y}}\Big|_k(\dot{y}_{k+1} - \dot{y}_k)$$

$$\frac{\partial\dot{\beta}}{\partial\dot{x}} = \frac{-y}{\rho^2}, \quad \frac{\partial\dot{\beta}}{\partial\dot{y}} = \frac{x}{\rho^2}$$

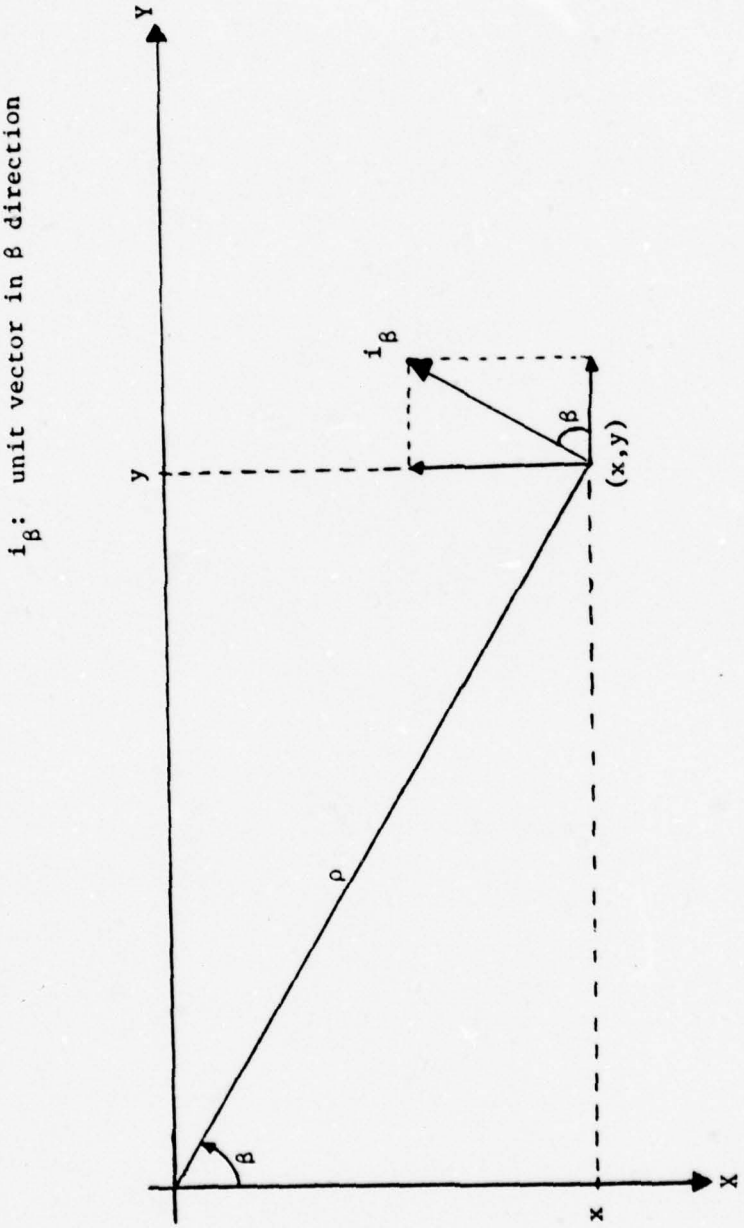

Figure 3. Direction cosines between i_β and the X and Y axes.

Using (12)

$$\dot{\beta}_{k+1} = \dot{\beta}_k + \left(\frac{-y}{\rho^2}\right)\Big|_k \left[E\dot{x}_k + Fw_{x_k}' + Au_{x_k} + Gw_{x_k} - \dot{x}_k \right]$$

$$+ \left(\frac{x}{\rho^2}\right)\Big|_k \left[E\dot{y}_k + Fw_{y_k}' + Au_{y_k} + Gw_{y_k} - \dot{y}_k \right]$$

$$= \dot{\beta}_k + E\left[\left(\frac{-y\dot{x} + x\dot{y}}{\rho^2}\right)\right]_k + F\left[\left(\frac{-y}{\rho}\right)w_x' + \left(\frac{x}{\rho}\right)w_y'\right]_k/\rho_k$$

$$+ A\left[\left(\frac{-y}{\rho}\right)u_x + \left(\frac{x}{\rho}\right)u_y\right]_k/\rho_k + G\left[\left(\frac{-y}{\rho}\right)w_x + \left(\frac{x}{\rho}\right)w_y\right]_k/\rho_k$$

$$- \left[\frac{-y\dot{x} + x\dot{y}}{\rho^2}\right]_k$$

From equation (24), the first and last terms on the right side of the above equality cancel. Hence using equation (26)

$$\dot{\beta}_{k+1} = E\dot{\beta}_k + F(w_\beta'/\rho)_k + A(u_\beta/\rho)_k + G(w_\beta/\rho)_k \tag{28}$$

A discrete-time model similar to equation (15) is used to describe w_β':

$$w_{\beta'}{}_{k+1} = e^{-at} w_{\beta_k}' + \frac{1}{a}(1 - e^{-aT}) w_{\beta_k} \tag{29}$$

Equations (27), (28), and (29) collectively form the following state variable model in the bearing plane:

$$\begin{bmatrix} \beta \\ \dot{\beta} \\ w_\beta' \end{bmatrix}_{k+1} = \begin{bmatrix} 1 & A & (B/\rho_k) \\ 0 & E & (F/\rho_k) \\ 0 & 0 & e^{-at} \end{bmatrix} \begin{bmatrix} \beta \\ \dot{\beta} \\ w_\beta' \end{bmatrix}_k + \begin{bmatrix} (C/\rho_k) \\ (A/\rho_k) \\ 0 \end{bmatrix} u_{\beta_k} + \begin{bmatrix} (D/\rho_k) \\ (G/\rho_k) \\ J \end{bmatrix} w_{\beta_k} \tag{30}$$

where

$$\rho = (x^2 + y^2)^{1/2}.$$

Equations (16), (23), and (30) constitute the range, elevation and bearing channels respectively, of the linearized spherical model for a maneuvering target. It is observed that there is slight coupling between the 3 channels insofar as the elevation channel requires the range estimate and the bearing channel the range and elevation estimate to compute ρ.

It should be noted here that the three state variable models (16), (23) and (30) are the result of incorporating the Singer correlated acceleration process into the linearized spherical model disclosed in [2].

Summary of (16), (23) and (30):

$$\begin{bmatrix} r \\ \dot{r} \\ w'_r \end{bmatrix}_{k+1} = \begin{bmatrix} 1 & A & B \\ 0 & E & F \\ 0 & 0 & e^{-aT} \end{bmatrix} \begin{bmatrix} r \\ \dot{r} \\ w'_r \end{bmatrix}_k + \begin{bmatrix} C \\ A \\ 0 \end{bmatrix} u_{r_k} + \begin{bmatrix} D \\ G \\ J \end{bmatrix} w_{r_k} \tag{16}$$

$$\begin{bmatrix} e \\ \dot{e} \\ w'_e \end{bmatrix}_{k+1} = \begin{bmatrix} 1 & A & (B/r_k) \\ 0 & E & (F/r_k) \\ 0 & 0 & e^{-aT} \end{bmatrix} \begin{bmatrix} e \\ \dot{e} \\ w'_e \end{bmatrix}_k + \begin{bmatrix} C/r_k \\ A/r_k \\ 0 \end{bmatrix} u_{e_k} + \begin{bmatrix} D/r_k \\ G/r_k \\ J \end{bmatrix} w_{e_k} \tag{23}$$

$$\begin{bmatrix} \beta \\ \dot{\beta} \\ w'_\beta \end{bmatrix}_{k+1} = \begin{bmatrix} 1 & A & (B/\rho_k) \\ 0 & E & (F/\rho_k) \\ 0 & 0 & e^{-aT} \end{bmatrix} \begin{bmatrix} \beta \\ \dot{\beta} \\ w'_\beta \end{bmatrix}_k + \begin{bmatrix} (C/\rho_k) \\ (A/\rho_k) \\ 0 \end{bmatrix} u_{\beta_k} + \begin{bmatrix} (D/\rho_k) \\ (G/\rho_k) \\ J \end{bmatrix} w_{\beta_k} \tag{30}$$

With the development of the spherical model now complete, attention will next be directed to the adaptive tracking filter.

ADAPTIVE TRACKING FILTER IN SPHERICAL COORDINATES

The adaptive portion of the tracking filter is concerned with modeling the unknown control input to the target. However, a brief case study is first required since the filter proposed here is an outgrowth of that disclosed by Moose/Gholson [2].

In the tracking filter reported by Moose/Gholson the input is viewed as coming from a set of N discrete levels $u^{(i)}$, $i = 1, 2, \ldots, N$. The maneuvering target is then represented as a "random switch" which arbitrarily selects the target input from among this set. By utilizing the semi-Markov [3] properties of this random switching, a set of N probabilities W_i, $i = 1, 2, \ldots, N$ is computed, where W_i is the probability that the current input being selected is $u^{(i)}$. Next a weighted sum of these inputs

$$\hat{u} = \sum_{i=1}^{n} u^{(i)} W_i \tag{31}$$

is computed and this quantity $\hat{u}$ forms the "deterministic input" to the Kalman filter. However, in order for this method to work effectively, many levels must be utilized. If an input is chosen which is not exactly "matched" to one of the discrete levels, a bias develops in the filter estimates. This bias can only be reduced at the expense of increasing the number of discrete levels to such an extent as to insure that a given input to the target will not be distant from one of these levels.

In an attempt to eliminate the bias problem arising from mismatched inputs the correlated Gaussian random process disclosed by Singer [1] was incorporated into the Moose/Gholson filter, as disclosed in the

previous section. The resulting estimator consisted of three Kalman filter algorithms based on equations (16), (23) and (30) for the r, e and β channels, respectively, with u_r, u_e and u_β being replaced by weighted estimates (31) of these inputs, namely $\hat{u}_r$, $\hat{u}_e$ and $\hat{u}_\beta$ using the semi-Markov statistics. Figure 4 is a block diagram of the elevation channel of this modified filter. Figure 5 shows the results obtained from the r(radial) channel of this filter on the following target trajectory.

Using a sampling period T = 0.3 sec, a drag coefficient $\alpha = 0.4$ and a correlated process with a standard deviation $\sigma_c = 30$ ft/sec^2 and correlated time constant $\tau_c = 10$ secs, the modified filter was exercised using synthetic data on a target initially retreating at a radial velocity of MACH 1·5 which subsequently turns around and approaches at a radial velocity of -MACH 1·5.

The insert below the graph in Figure 5 clearly shows the extent of the mismatch which exists between the levels of the applied control sequence (dashed lines) and the discretized levels used in the filter (solid lines).

The estimated target radial velocity (dashed lines) is seen to have large oscillations about the true radial velocity (solid line). The oscillations result from the "states" not being adequately separated in the state space for consistent convergence of the probabilities W_i to the correct level. This point will be expanded on in the next section; suffice it to say here that this inconsistency in the probabilities causes the estimate $\hat{u}_r$ to be biased off a substantial amount from the actual target input. This alternate biasing to the right and then to the left of the actual target input causes the estimates to alternate from being too large to being too small.

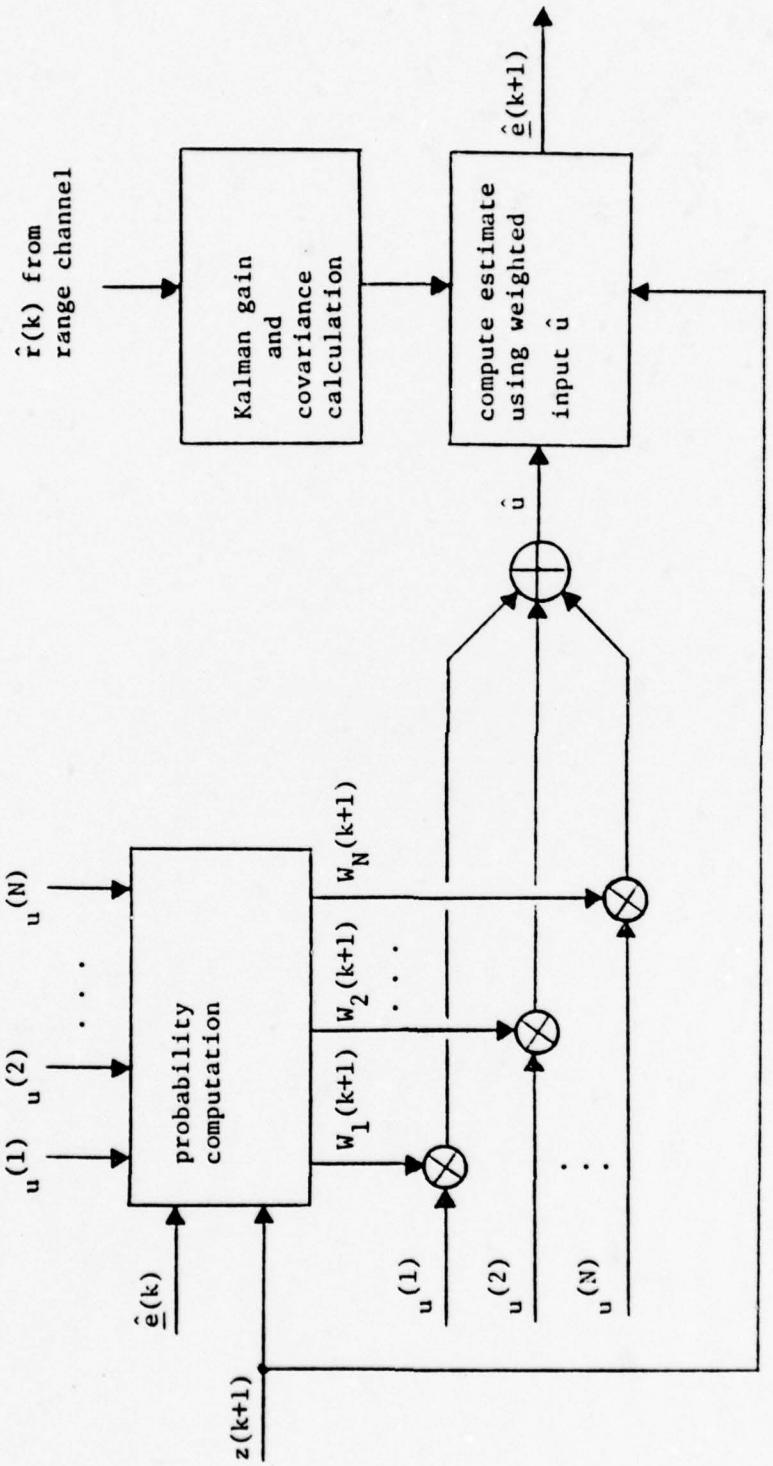

Figure 4. Block diagram of the elevation channel of the Moose/Gholson filter.

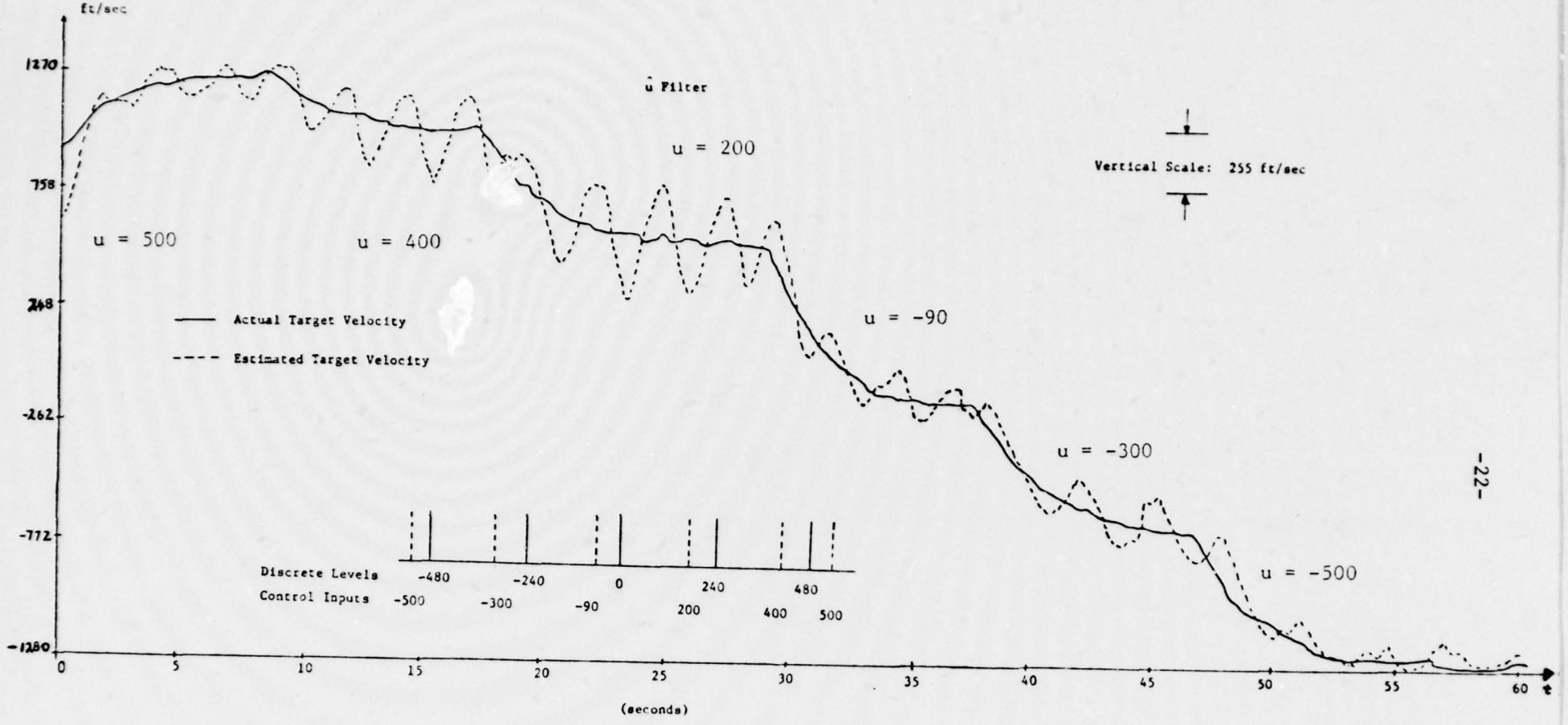

Figure 5. Radial velocity tracking by the Moose/Gholson filter incorporating the Singer correlated process.

In the following solution to this problem, explicit reference is made to the radial channel, for convenience; however, it should be understood that a similar analysis holds true for both the elevation and bearing channels.

The heart of the adaptive filter proposed in this report is in *the forming of the estimate of the target states (in each channel) from a weighted sum of estimates conditioned on the N individual discrete levels, rather than by forming a weighted sum of the N discrete levels first and then computing the estimate. This difference can easily be seen by comparing Figures 4 and 7.*

To this end consider the state model (16). This state model views the target input acting in the radial direction as being derived from a correlated Gaussian density having a mean value u_r. Next consider a series of N such Gaussian curves with displaced mean values $u_r^{(i)}$, $i = 1, 2, \ldots, N$ and partially overlapping "tails" as shown in Figure 6. If a bank of N Kalman filters is formed, each filter based on (16) with the deterministic input u_r being a different one of these N mean values, then a series of N estimates is obtained, each conditioned on a different Gaussian curve of Figure 6. Next a weighted sum of these estimates is obtained in a manner to be disclosed below, and this weighted sum is taken to be the unconditioned estimate of the target states.

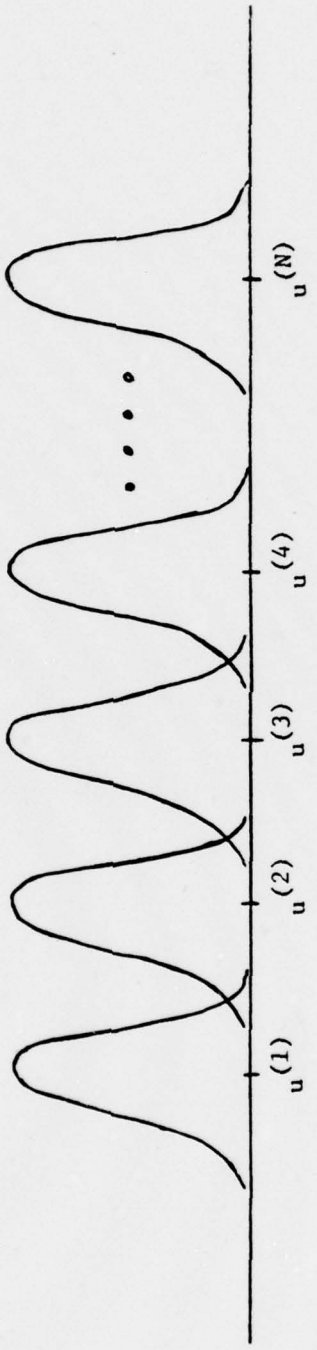

Figure 6. Series of N partially overlapping Gaussian curves.

Calculation of weighting coefficients:

As has been disclosed, the target input is viewed as coming from one of N possible overlapping Gaussian curves each of which has a predetermined mean value. As the target executes a series of evasive maneuvers in the radial channel, for example, the changing input to produce these maneuvers is now viewed as randomly switching among these N curves. By applying the semi-Markov statistics to this switching process a series of N probabilities W_i, $i = 1, 2, \ldots, N$ is generated where

$$W_i \equiv \Pr \{\text{target input is being derived from the Gaussian curve whose mean value is } u_r^{(i)}\}.$$

These W_i are then used to form the weighted estimate.

Before deriving the recursive form for W_i, $i = 1, 2, \ldots, N$ it should first be pointed out again that each of the separate signal channels is independent in the sense that the processing of a given channel depends only on past estimates in a parameterized manner. For instance, the elevation channel carries on its processing of the elevation measurements dependent on the other channels only to the extent that the previous range estimate is required as a parameter in the elevation channel transition matrices. Because of this decoupled property of the algorithm, the estimation algorithm for a single (elevation) channel need only be described, the other channels (range and bearing) being similar.

We begin with the well-known relation that the optimal estimate of the elevation signal can be written as a weighted sum of the input-conditioned estimates. Thus, if $\hat{e}^{(i)}(k + 1)$ represents the optimal estimate of $e(k + 1)$ given that the ith input force $u^{(i)}$ is present

(the ith-input force being one of the previously described mean values), then based on the data sequence

$$Z(k+1) = \{z(1), z(2), \ldots, z(k), z(k+1)\},$$

we define

$$\hat{e}(k+1) = \sum_{i=1}^{N} \hat{e}^{(i)}(k+1)\, W_i(k+1) \tag{32}$$

where

$$W_i(k+1) = \Pr\{u(k) = u^{(i)} | Z(k+1)\} \tag{33}$$

and

$$\hat{e}^{(i)}(k+1) = E\{e(k+1) | u(k) = u^{(i)}, Z(k+1)\}.$$

Equation (32) is a total probability expression developed from the basic relation that

$$\hat{e}(k+1) = E\{e(k+1) | Z(k+1)\}$$

is the optimal mean-squared estimate. It is well known that the optimal input-conditioned estimates are provided by suitably matched Kalman filters. In particular,

$$\hat{e}^{(i)}(k+1) = \Phi(k)\, \hat{e}^{(i)}(k) + \Gamma(k)\, u^{(i)} + K(k+1)\, [z(k+1) - H\Phi(k)\, \hat{e}^{(i)}(k) - H\Gamma(k)\, u^{(i)}] \tag{34}$$

where

$$M(k+1) = \Phi(k)\, P(k)\, \Phi^{T}(k) + \Psi(k)\, Q\Psi^{T}(k) \tag{35}$$

$$K(k + 1) = M(k + 1)\ H^T[HM(k + 1)\ H^T + R]^{-1}, \tag{36}$$

and

$$P(k + 1) = [I - K(k + 1)H]\ M(k + 1). \tag{37}$$

The matrices Φ, Γ and Ψ are used to denote the respective coefficient matrices in (23); in addition, due to the spherical approximation the measurement matrix assumes the simple form (for each channel)

$$H = [1 \quad 0 \quad 0].$$

The following is an outline of the analysis given in [3] to calculate the recursive weighting coefficients W_i, $i = 1, 2, \ldots, N$. Defining $Z(k + 1) = \{Z(k), z(k + 1)\}$, apply Bayes Theorem to (33) and obtain

$$W_i(k + 1) = \frac{\Pr\{u(k) = u^{(i)} | Z(k)\}\ p\{z(k + 1) | u(k) = u^{(i)}, Z(k)\}}{p\{z(k + 1) | Z(k)\}} \tag{38}$$

The denominator is independent of i and is therefore common to each $W_i(k + 1)$ as a normalizing constant. The first numerator factor of (38) is determined from the semi-Markov input process. Expanding this factor in a total probability expression

$$\Pr\{u(k) = u^{(i)} | Z(k)\} = \sum_{j=1}^{N} \Pr\{u(k) = u_i | u(k - 1) = u_j, Z(k)\} W_j(k).$$

And since Z(k) has no influence on the Markov state transitions,

$$\Pr\{u(k) = u^{(i)} | Z(k)\} = \sum_{j=1}^{N} \theta_{ji}\ W_j(k) \tag{39}$$

where

$$\theta_{ji} = \Pr\{u(k) = u_i | u(k - 1) = u_j\}$$

Combining (38) and (39)

$$W_i(k+1) = C_1\, p\{z(k+1) \mid u(k) = u^{(i)},\, Z(k)\} \sum_{j=1}^{N} \theta_{ji}\, W_j(k) \qquad (40)$$

is the desired recursive relation for W_i. The required density p is approximately normally distributed and has distribution

$$P\{z(k+1) \mid u(k) = u^{(i)},\, Z(k)\} \sim N\{m_i(k+1),\, C_i(k+1)\}, \qquad (41)$$

where

$$m_i(k+1) = H[\Phi(k)\, \hat{e}^{(i)}(k) + \Gamma(k)\, u^{(i)}(k)] \qquad (42)$$

and

$$C_i(k+1) = [HM(k+1)\, H^T + R] \qquad (43)$$

The final estimation algorithm consists of the calculations implied by (34), (41), (42), (43), (39), (40) and (32).

With the derivation of the adaptive estimator now complete, several comments are in order.

The use of the word "optimal" in the previous analysis needs to be qualified for the following two reasons:

(1) Since the target input is usually unknown when using actual radar data, the above modeling of this unknown input is at best approximate and generally does not match the true target input from iteration to iteration. Indeed, being cognizant of this mismatch, the Singer process was incorporated to raise

the estimator uncertainty concerning the input and in this manner to produce improved estimates. In reference [4] it is shown that one additional covariance term is also needed to account for this mismatch.

(ii) When a target maneuver occurs, the weighting coefficients do not respond immediately but rather have a finite learning time. Consequently, during this learning period the incorrect filter is being weighted the most while the filter closest to the new target configuration is being weighted by a small amount causing the estimates to lag the true target states.

Because of (i) and (ii) the adaptive estimator developed here must be considered sub-optimal.

Consider the measurement density conditioned on the ith mean value as given in (41). This density has covariance

$$C_i(k+1) = [HM(k+1)\ H^T + R] \tag{43}$$

where $M(k+1)$ is given by (35). What characterizes the different target "states" is the set of Gaussian curves used to model the switching input. However, the target dynamics remain the same for all the "states". Consequently, if the process and measurement noise covariances $Q(k+1)$ and $R(k+1)$, respectively, are assumed to remain constant as the target switches from one "state" to another, then none of the quantities on the right of (43) is conditioned on i. Under these conditions, for a given value of $(k+1)$, $C_i(k+1)$ has the same value for all values of $i = 1, 2, \ldots, N$. Indeed it is clear that for each value of $(k+1)$,

the entire covariance analysis is identical for each filter in the previously mentioned filter "bank". Therefore, the bank of filters may be reduced to a single filter for this segment of the algorithm.

Consider next augmenting both the state predict and state update estimate vectors of this single filter to form two N column matrices, the ith column of each matrix being the estimate conditioned on the ith mean value. If the scalar measurement residual is augmented to form an N element measurement residual vector, then this single "augmented" filter now produces a set of N conditioned estimates of the target states as if an entire bank of N filters had been executed. These N estimates are then weighted by the weighting coefficients (40) to yield an unconditioned estimate. A block diagram of this "augmented" filter is given in Figure 7.

The underlying causes of the oscillations in Figure 5 can now be explained. In equation (42), at time (k + 1) the mean value of the measurement conditioned on $u^{(i)}$ is seen to be a function of the quantities $\hat{e}^{(i)}(k)$ and $u^{(i)}(k)$. Both of these quantities have different values for each i and lead to a good discrimination among the $m_i(k)$. In the Moose/Gholson filter, the corresponding $m_i(k)$ has the value

$$m_i(k) = H[\Phi(k)\ \hat{e}(k) + \Gamma(k)\ u^{(i)}(k)] \tag{44}$$

In (44) $\hat{e}(k)$ has the same value for each i and only the quantity $u^{(i)}(k)$ is used to differentiate among the different $m_i(k)$. The improved filter performance resulting from the better discrimination afforded by (42) can be seen from Figure 8. The trajectory in this Figure is identical in every respect to that of Figure 5. As can be seen from the insert in

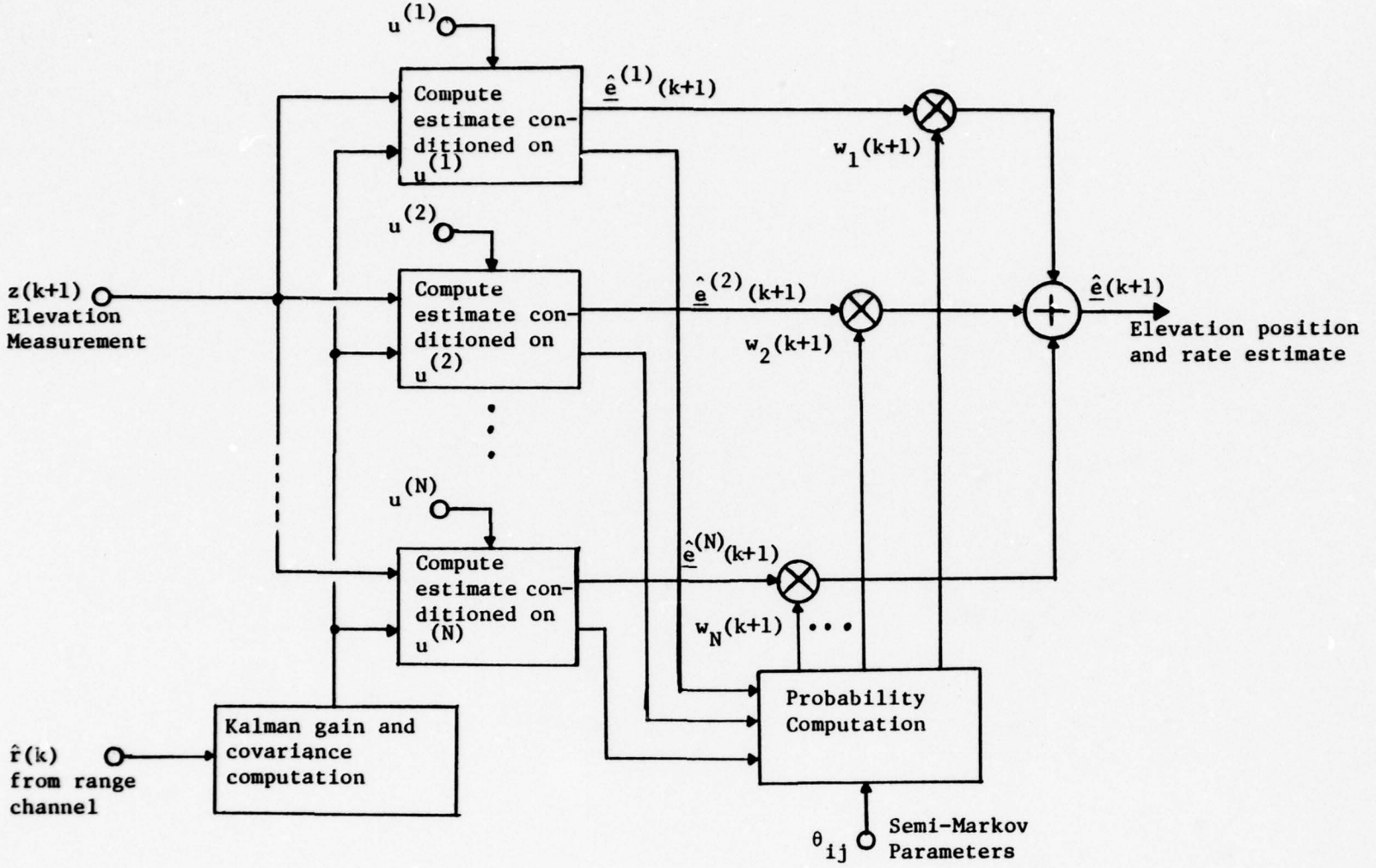

Figure 7. Elevation channel block diagram of the augmented filter.

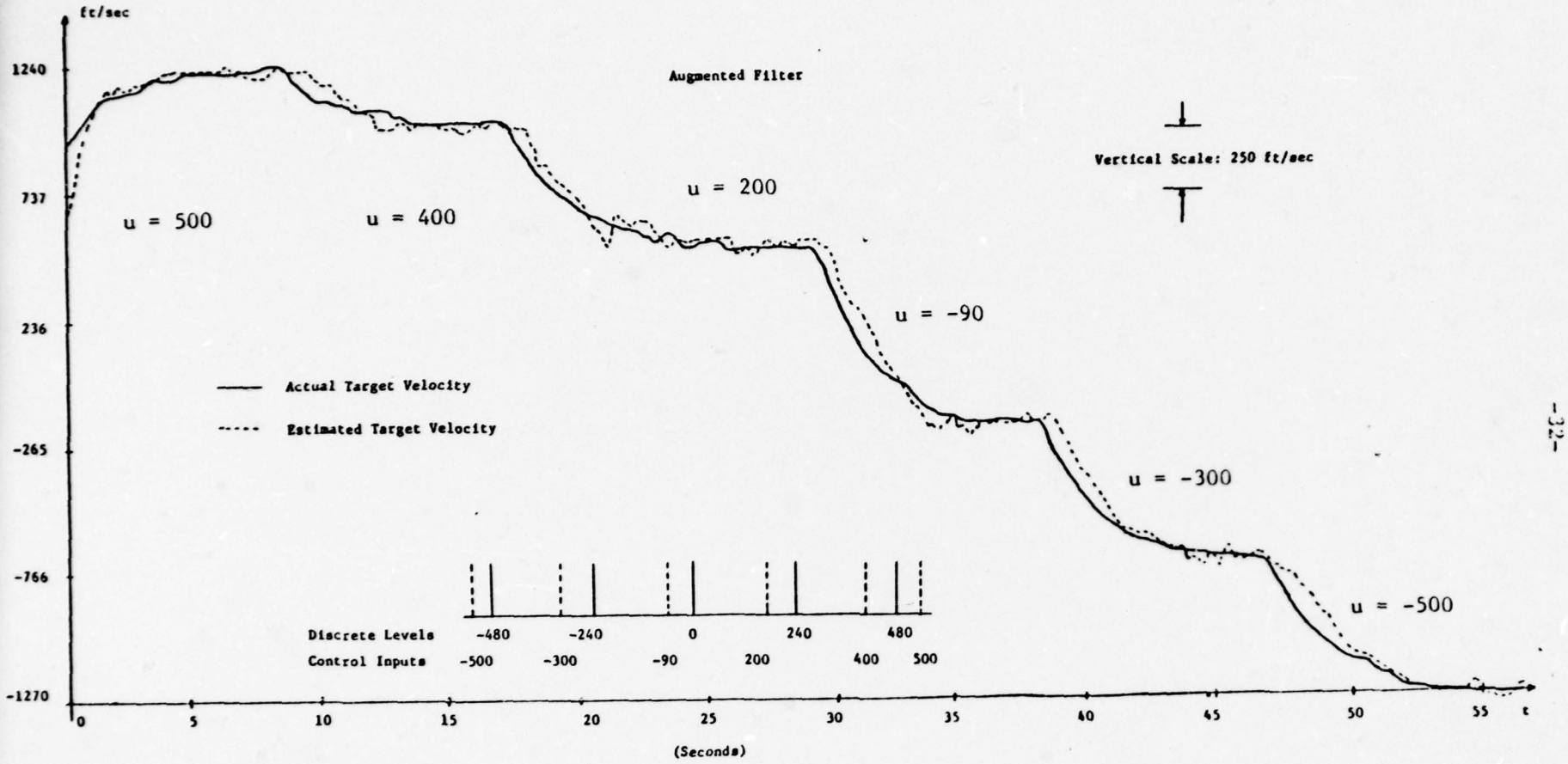

Figure 8. Radial velocity tracking by the augmented filter.

Figure 8, the mean values used in the augmented filter are also identical to those used in Figure 5; in addition process and measurement noise covariances were the same in both runs. The oscillations experienced in Figure 5 are seen to be absent in Figure 8. Maneuvers are detected sooner and the filter settling time is much shorter.

In the next section the design process used in assigning values to the various parameters in the augmented filter will be discussed. Following that the filter performance against actual air target radar data will be illustrated graphically from the point of view of the GUSS supplied SIG3D parameter.

PARAMETER SELECTION PROCESS FOR THE AUGMENTED FILTER

The parameter selection process concerns itself with the following parameter set

$$\{\alpha, \sigma_c, N, V_{max}, a\}$$

where

α is the assumed drag coefficient

σ_c is the standard deviation of the correlated process

N is the number of levels (mean values)

V_{max} is the assumed maximum possible speed of the target set to be tracked.

$a = 1/\tau_c$

The design process is given for the r channel. The parameter values calculated for the r channel are then used in the e and β channels.

Consider the state model (16). A continuous time differential equation for this model is given by

$$\ddot{r} = -\alpha\dot{r} + u_r + w_r'$$

$$\dot{w}_r' = -aw_r' + w_r$$

Concentrating on the deterministic part of this differential equation for the moment, and defining

$$V_r \equiv \dot{r}$$

we have that

$$\dot{V}_r = -\alpha V_r + u_r$$

In the steady state, when $\dot{V}_r = 0$, the following relationship exists between u_r and $V_{r_{ss}}$

$$u_r = \alpha V_{r_{ss}}$$

where $V_{r_{ss}}$ is the steady state value of V_r.

Therefore a bound on the maximum target velocity establishes a bound on the maximum value of u_r.

In the first version of the filter developed here, a bound of ±1,200 ft/sec was assumed for $\dot{r}$ (both signs are used to account for either a retreating or approaching target). In addition a value of $\alpha = 0.4$ was selected because this value produced a quick transient response indicative of a high speed air target dynamics.

With both of these parameters defined, the resulting bound on u_r is

$$-480.0 \leq u_r \leq +480.0$$

The remaining parameters σ_c and N are then chosen in such a way as to embrace the continuum of possible u_r values lying within this bound. For example, in the first version of the filter, a set of N = 5 Gaussian curves was chosen, with the following mean values

$$-480.0,\ -240.0,\ 0.0,\ 240.0,\ 480.0$$

each curve having a standard deviation of

$$\sigma_c = 30\ (\text{ft/sec}^2).$$

These values for N, σ_c and the discrete levels were arrived at empirically by exercising the filter against a variety of target trajectories and observing the overall quality of filter estimates.

The parameter $a = \frac{1}{\tau_c}$ where τ_c is the correlation time constant of the *Gaussian process* had the value

$$a = 0.1$$

in both filter versions. This value was suggested by Singer [1] for a maneuvering air target.

To summarize, the following set of parameters was used in the first version

$$\begin{aligned} T &= 0.25 \text{ seconds (sampling interval)} \\ \alpha &= 0.4 \\ \sigma_c &= 30\ (\text{ft/sec}^2) \\ N &= 5 \\ V_{max} &= \pm\ 1{,}200\ (\text{ft/sec}) \\ a &= 0.1 \end{aligned} \qquad (45)$$

mean values: -480, -240, 0, 240, 480

An identical set of parameters was used in the elevation and bearing channels. Incidentally the above values were also used in obtaining the results of Figure 8.

The choice of the parameter subset

$$\{N, \sigma_c\}$$

is essentially a tradeoff of one parameter against the other. For example, in the second version of the augmented filter the number of means values was increased to N = 17. This permitted a reduction of σ_c to 15 (ft/sec^2) in the r channel and to 25 (ft/sec^2) in the e and β channels. The smaller σ_c in the r channel from that used in the e and β channels was possible by recognizing that the target radial velocity is generally less than zero and consequently only non-positive mean values were necessary in this channel. The entire parameter set used in the modified augmented filter is summarized in (46) for convenience.

$$\begin{aligned} T &= 0.25 \text{ seconds (sampling interval)} \\ \alpha &= 0.4 \\ \sigma_c &= 15 \text{ (ft/sec}^2\text{) r channel} \\ &= 25 \text{ (ft/sec}^2\text{) e and } \beta \text{ channels} \\ N &= 17 \\ V_{max} &= -1{,}200 \text{ (ft/sec)} \\ a &= 0.1 \end{aligned} \tag{46}$$

Means values: 0, -30, -60, -90, -120, . . . , -480 (r channel)

-480, -420, -360, -300, . . . , 480 (e and β channels)

The above analysis shows that the parameter selection process is essentially trial and error and consequently no claim is being made concerning optimality.

COMPARISON OF THE GIP AND AUGUMENTED FILTER USING ACTUAL RADAR TRAJECTORY DATA

The remaining part of this report is devoted to a comparison of the augmented filter and the three-dimensional rectangular GIP filter. This comparison takes the form of a series of graphs, one for each trajectory, each graph having three superimposed plots. Two of these plots refer to the augmented filter and the third to the GIP filter. The plots labeled "5 levels" and "17 levels" refer to the augmented filters having the parameter sets (45) and (46), respectively.

Each plot shows the variation of the GUSS supplied SIG3D parameter versus range for the associated filter; by superimposing three plots a convenient visual comparison of the relative filter performance is produced for each trajectory run. Since this SIG3D parameter represents an index of the standard deviation of the three-dimensional error in the aim point for a shell fired at the target, any decrease in this parameter's value is highly desirable.

The graphs show a consistently smaller value for SIG3D produced by the "17 level" filter as compared to that produced by the "5 level" filter, for all values of range. The difference between both of these values and the corresponding SIG3D produced by the GIP filter is quite large, the latter at times being several orders of magnitude larger for targets at distant ranges.

In an attempt to evaluate the relative reduction in the SIG3D parameter individually contributed by the spherical filter and the spherical predictor, the following series of tests were performed. The set of trajectories in Figures 9 thru 15 were run again, this time using the rectangular GIP predictor in conjunction with the spherical filter.

Overall, these tests indicated that the relative importance of filter and predictor is trajectory dependent. Several trajectories showed only a slight deterioration in the SIG3D parameter using the rectangular predictor while in others the deterioration was quite significant.

One of the latter cases--trajectory #119-- is shown in Figure 16. In this figure, the SIG3D parameter using the rectangular predictor is considerably larger than the corresponding values for the spherical predictor, for ranges in excess of 2.0 K yards. In view of these results, therefore, it appears that for fire control purposes the spherical predictor is the preferred one since it yields consistently better results over a broad spectrum of trajectories.

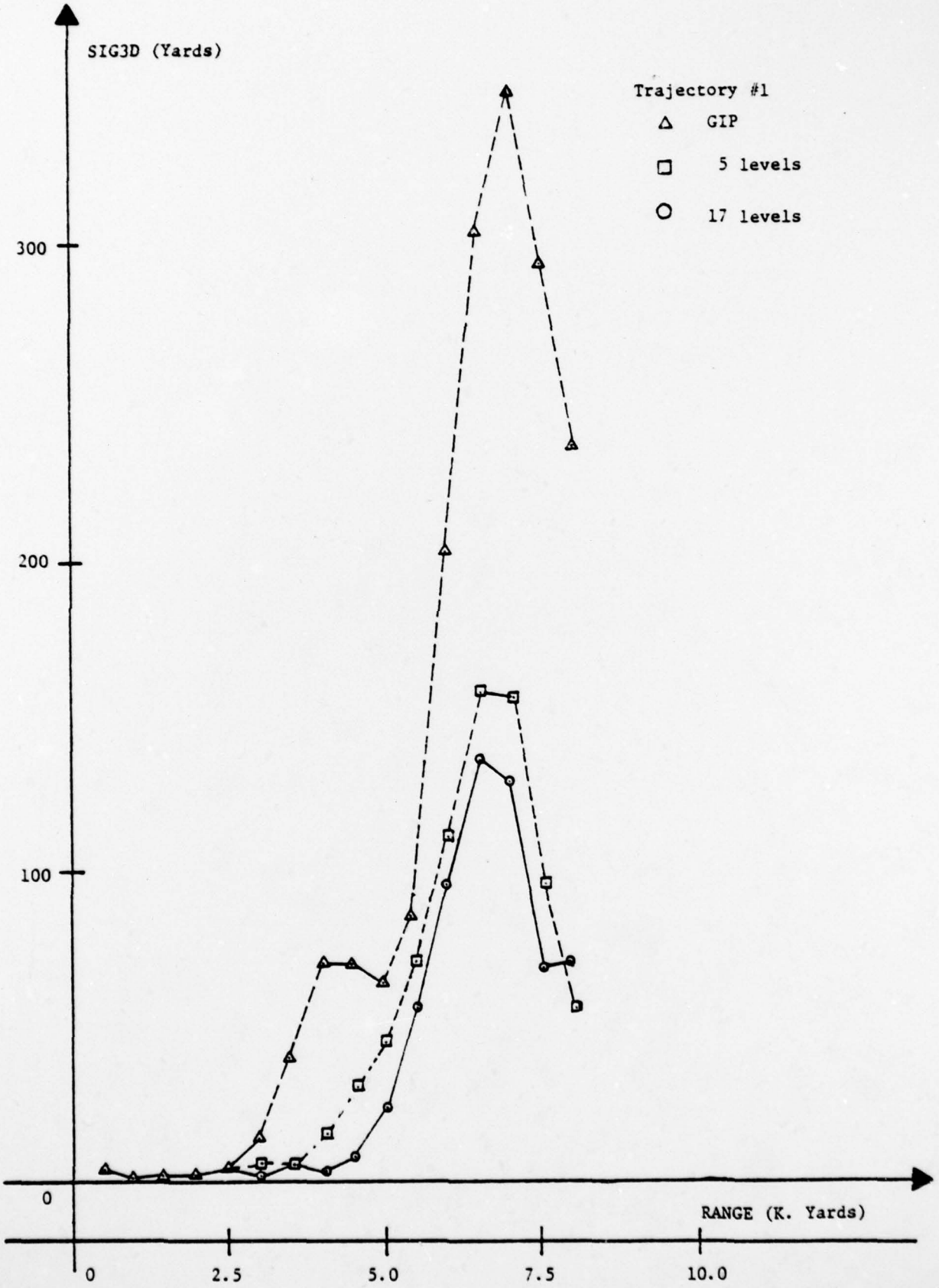

Figure 9. SIG3D versus range for trajectory #1.

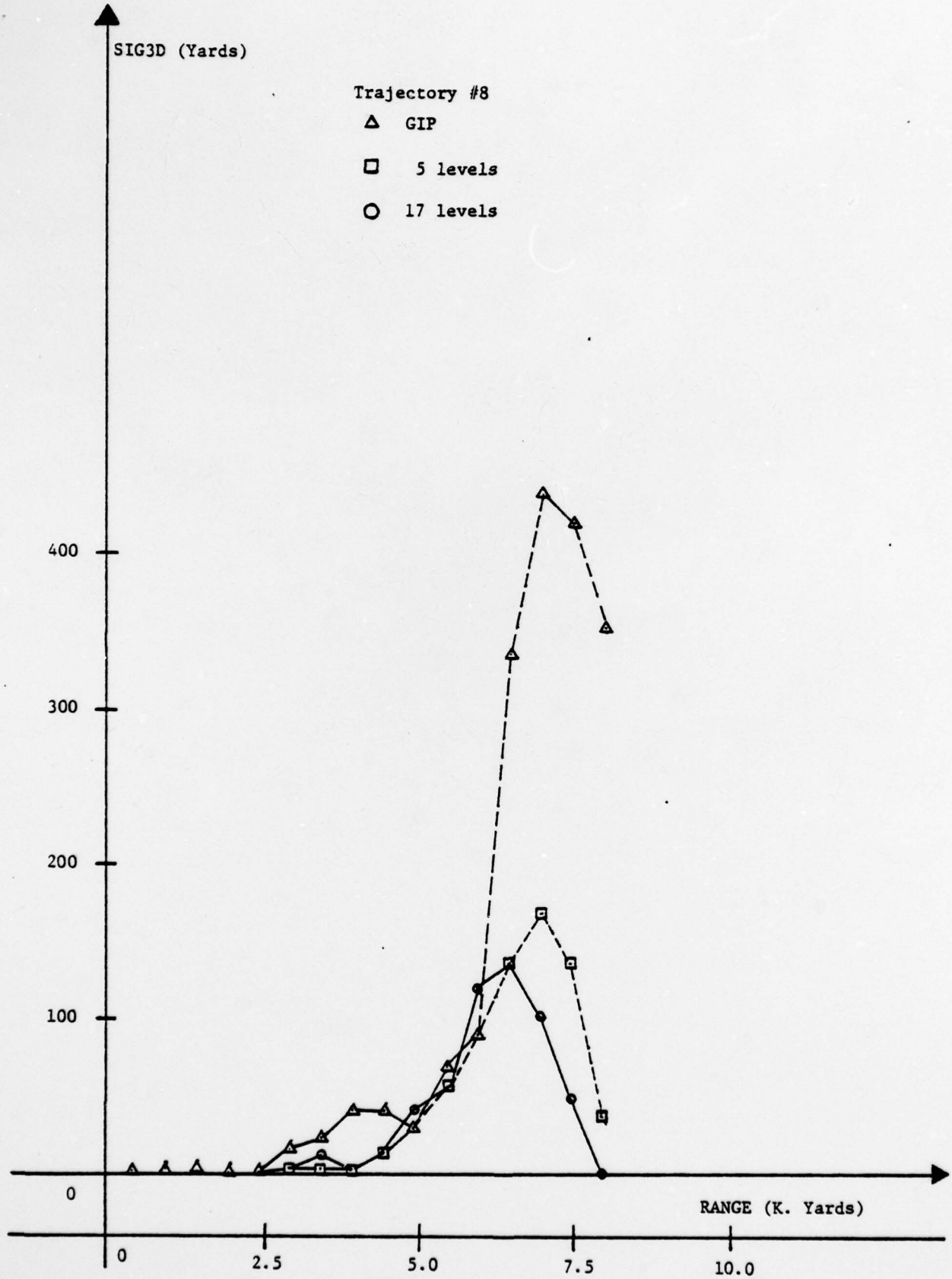

Figure 10. SIG3D versus range for trajectory #8.

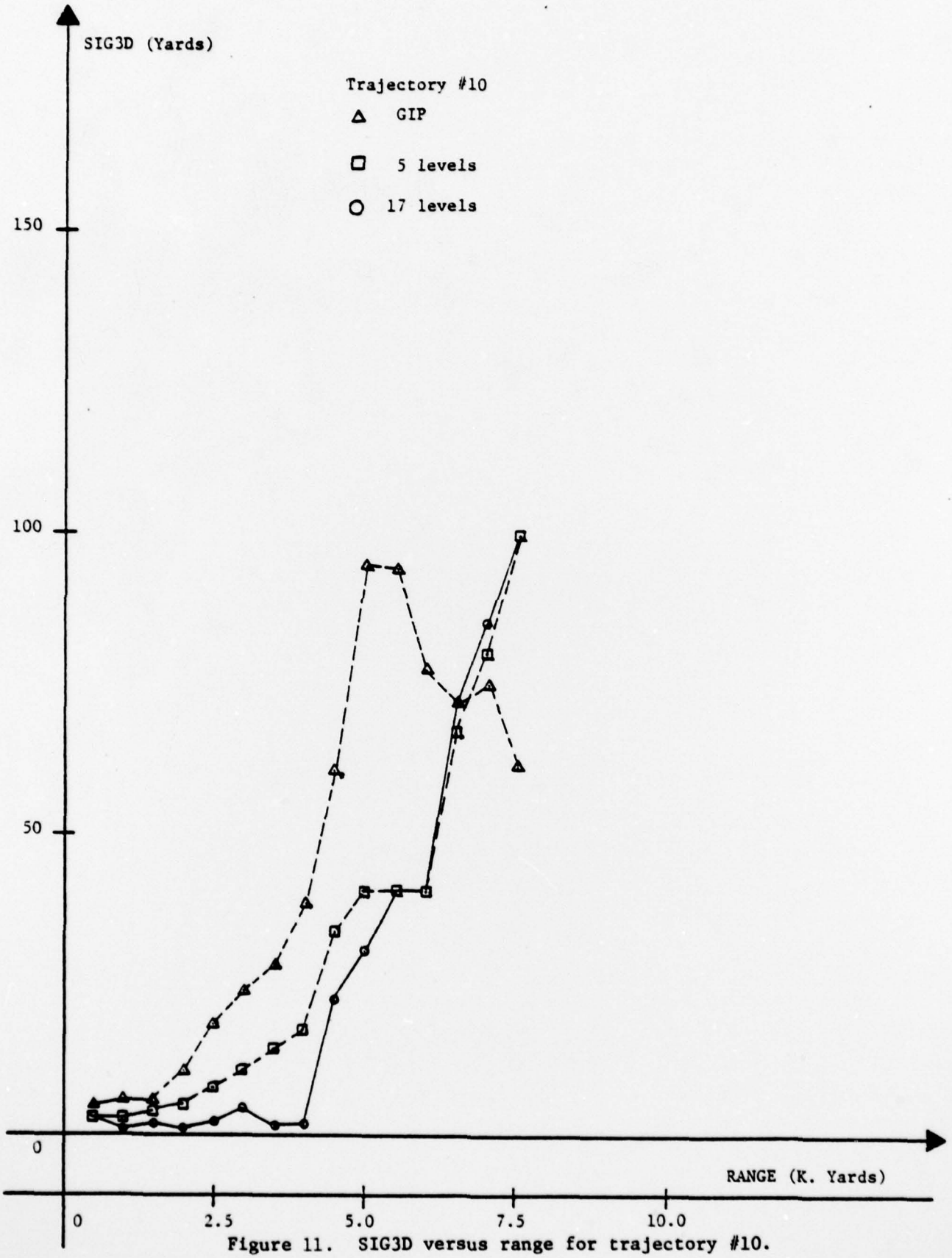

Figure 11. SIG3D versus range for trajectory #10.

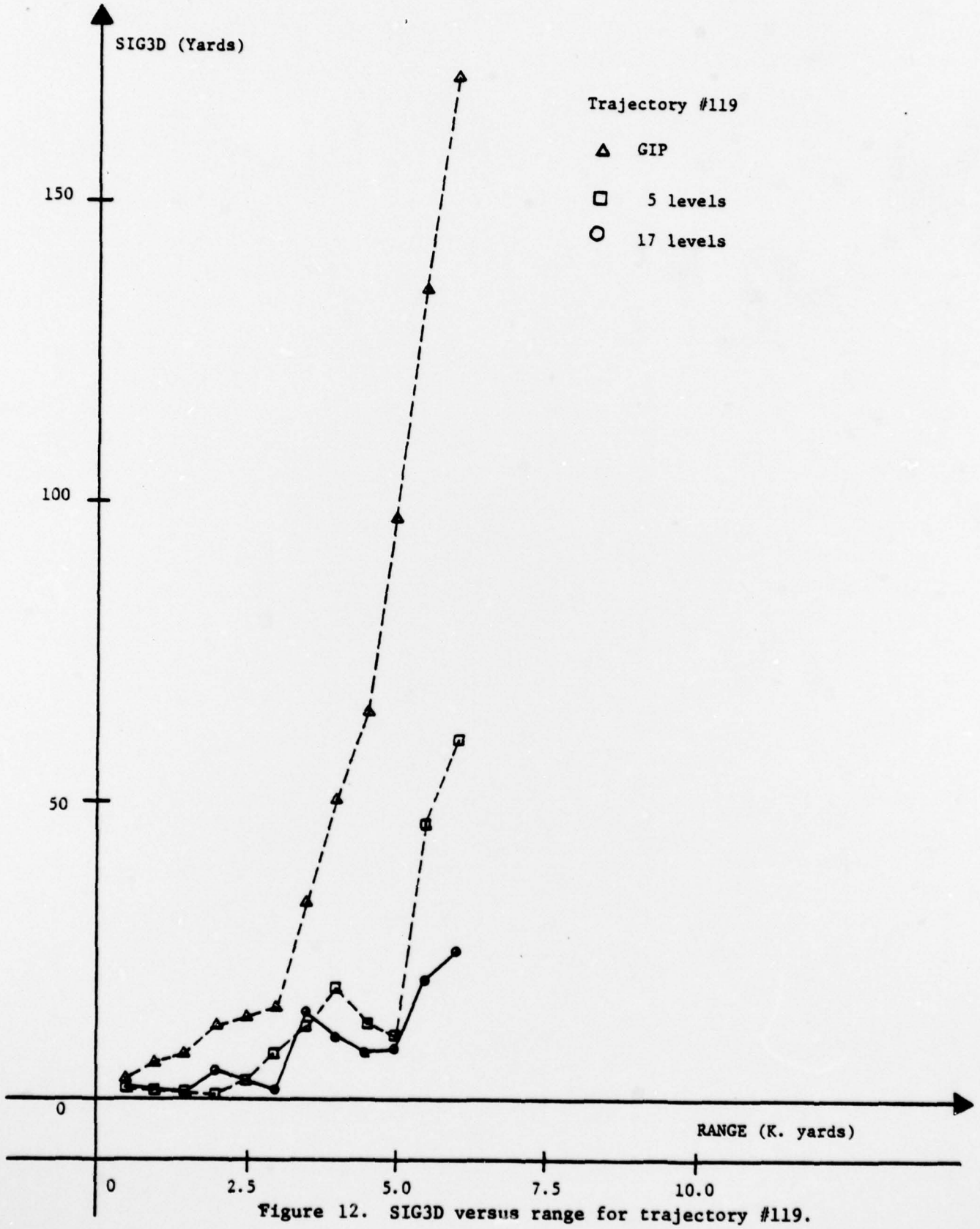

Figure 12. SIG3D versus range for trajectory #119.

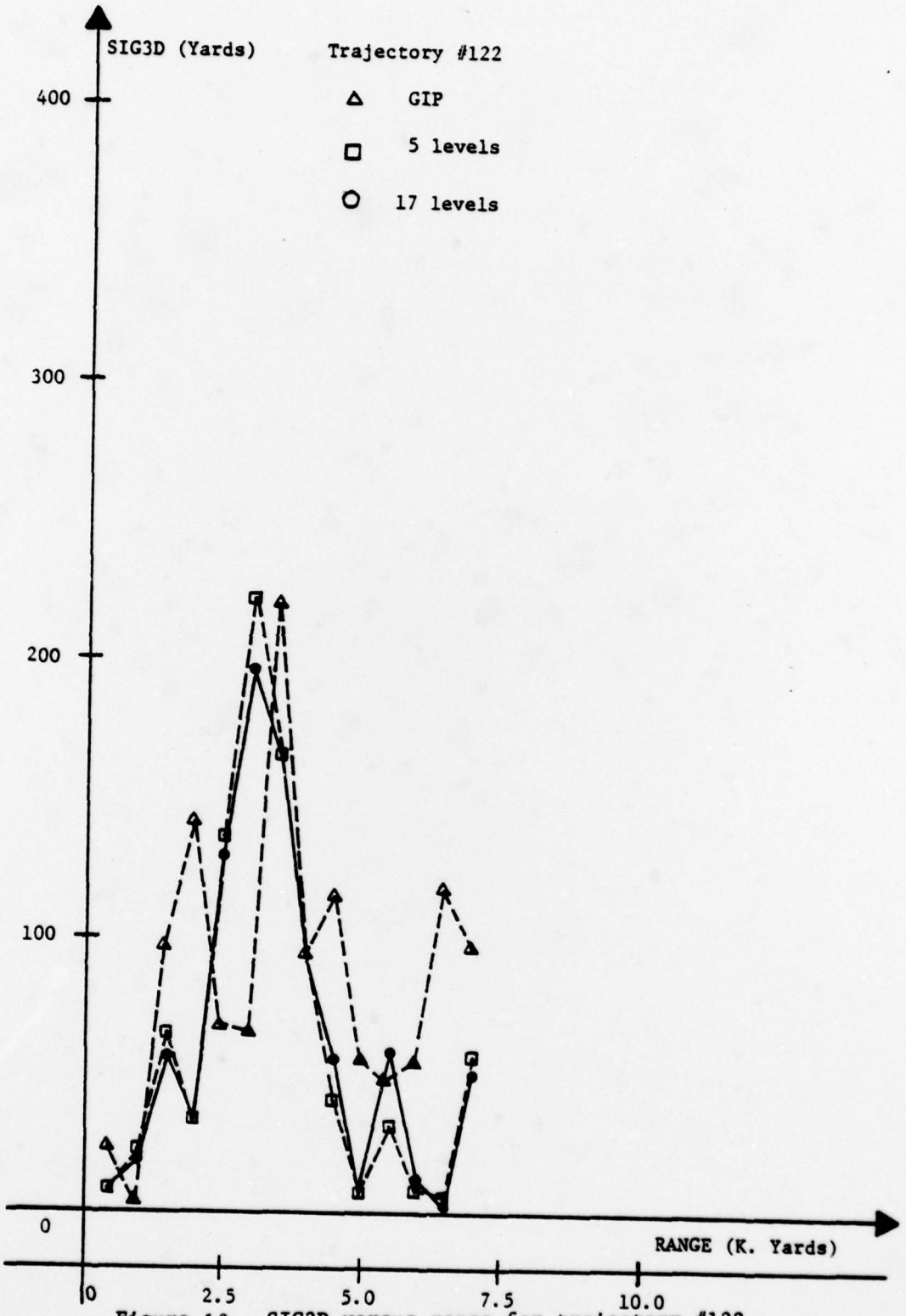

Figure 13. SIG3D versus range for trajectory #122.

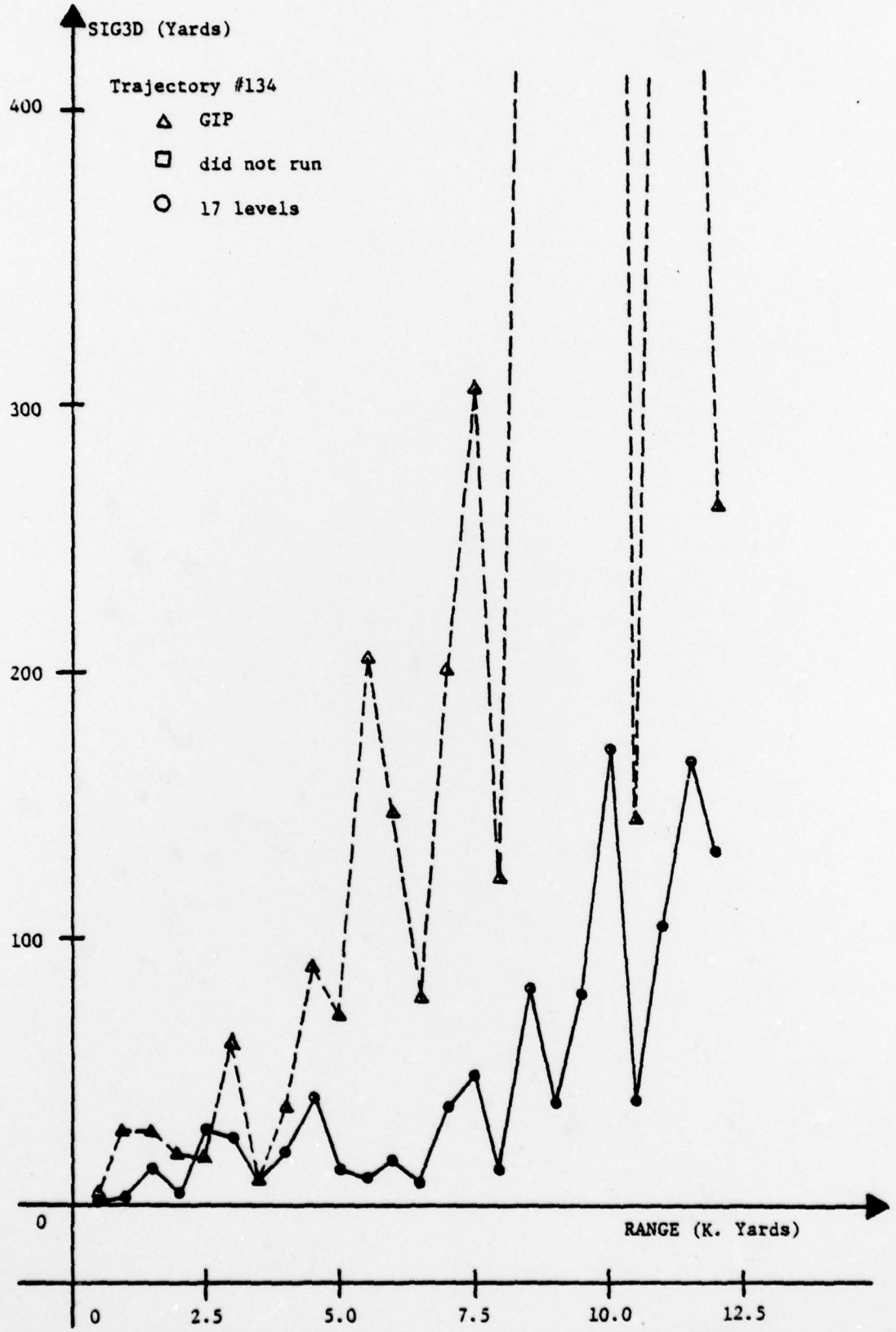

Figure 14. SIG3D versus range for trajectory #134.

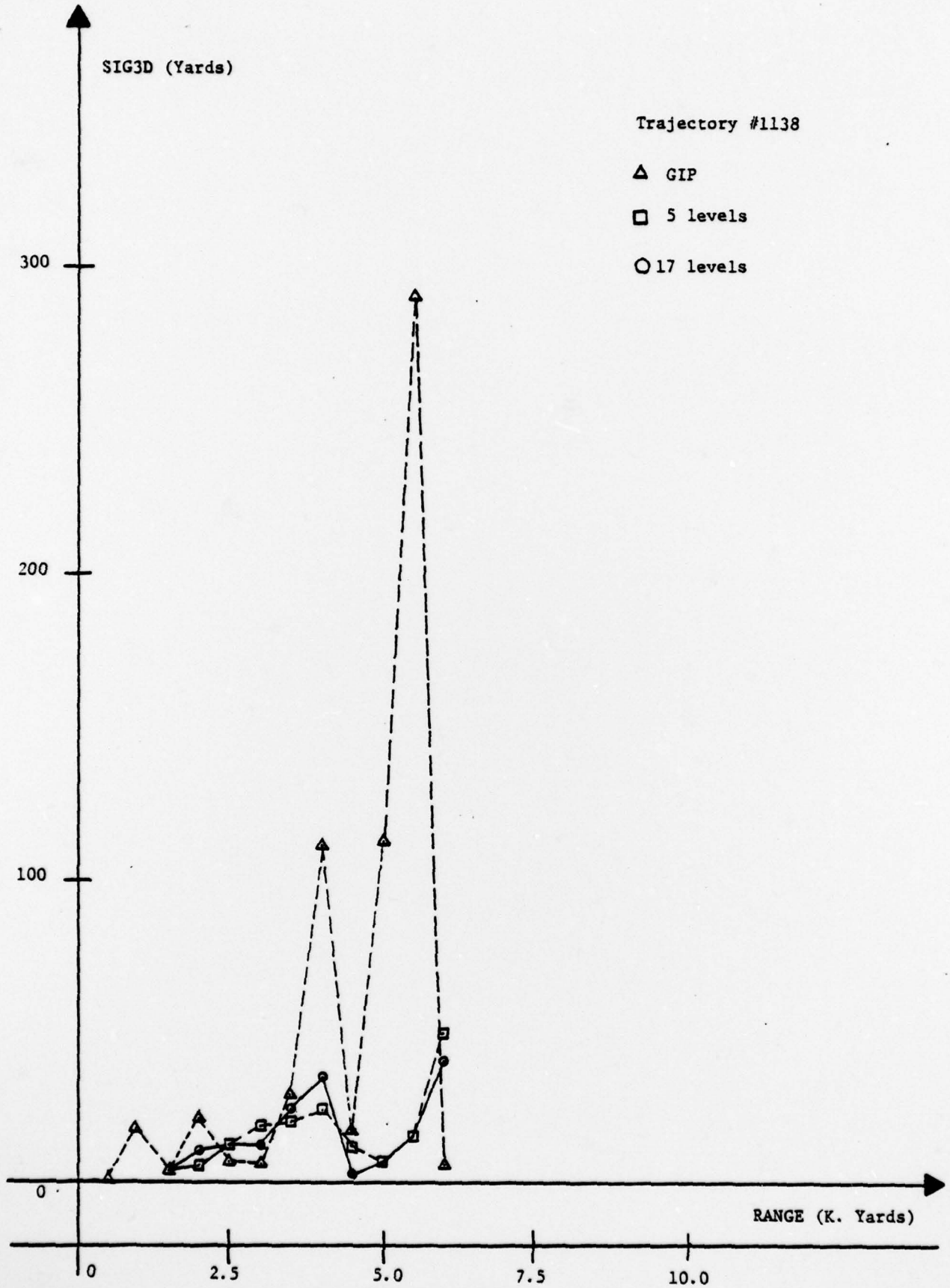

Figure 15. SIG3D versus range for trajectory #1138.

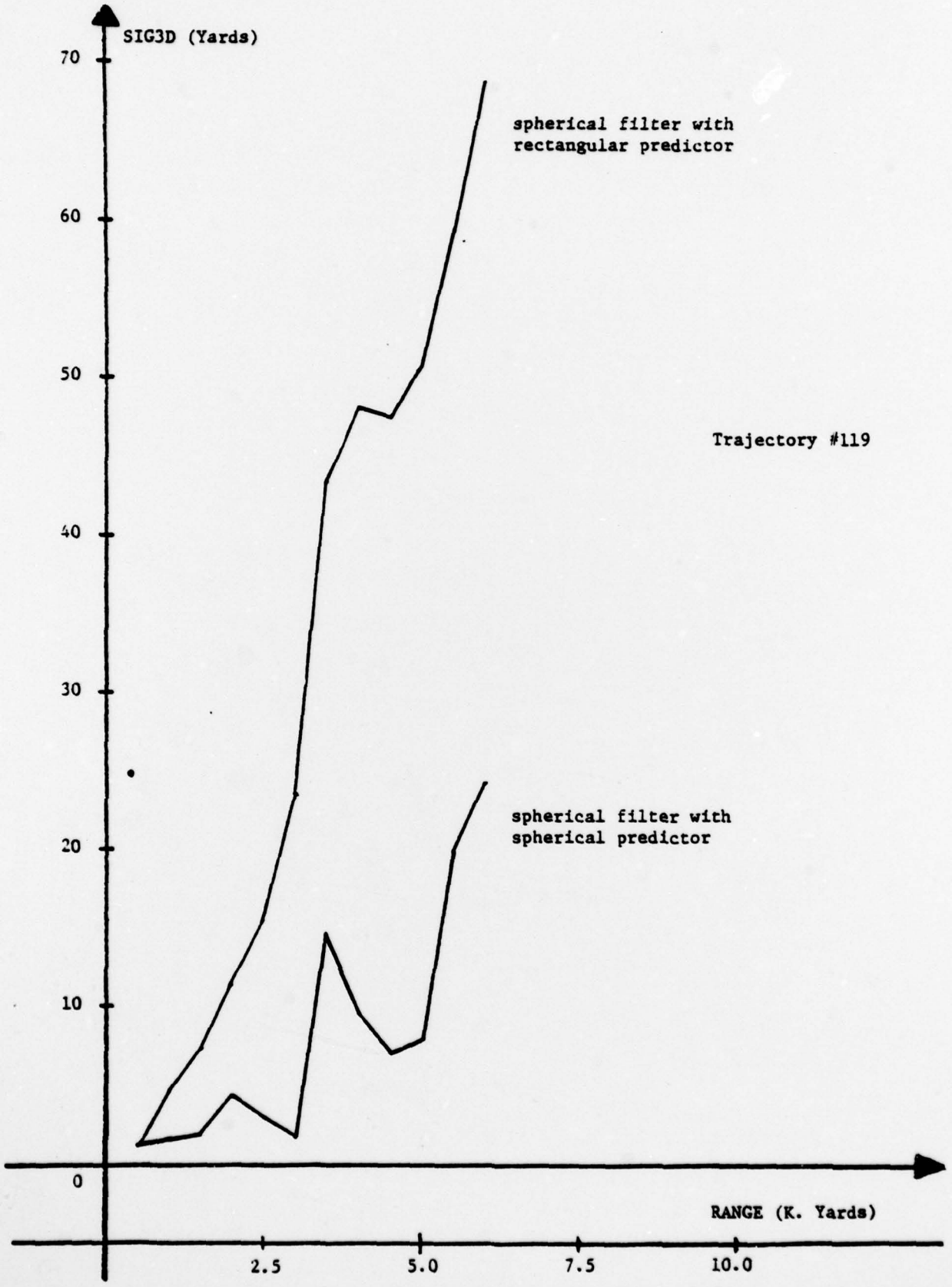

Figure 16. Comparison of rectangular and spherical fire control predictors.

CONCLUSION

By modeling a maneuvering air target in spherical coordinates, a simplified three dimensional "augmented" tracking filter algorithm has been developed. This filter when combined with a spherical constant velocity fire control predictor yields, for all target ranges, both a consistently higher probability of kill together with a smaller value for the SIG3D parameter than those produced by the GIP filter. These results were obtained on a variety of air target trajectories.

The simplification in the filter was made possible by the linear constant coefficient measurement matrix H which not only has obviated the use of the Extended Kalman filter, but also has permitted to a great degree the decoupling of the range, elevation and bearing channels.

In a separate series of tests on these trajectories to determine the relative merits of the rectangular GIP predictor versus the spherical predictor, it was found that the spherical predictor generally yielded better results and is to be preferred.

While the results of this report indicate an improvement by increasing from 5 to 17 the number of levels of the augmented filter, such an increase cannot be carried out indefinitely. As the number of levels increase, the process noise variance becomes vanishingly small and the filter becomes less able to respond to a change in maneuver level. Of course this increase also imposes a higher computational load.

REFERENCES

[1] R. A. Singer, "Estimating optimal tracking filter performance for manned maneuvering targets," IEEE Trans. Aerosp. Electron. Syst., July 1970.

[2] N. H. Gholson, and R. L. Moose, "Maneuvering Target Tracking Using Adaptive State Estimation," IEEE Trans. on Aerospace and Electronic Systems, May 1977.

[3] R. L. Moose and P. O. Wang, "An Adaptive Estimator with Learning for a Plant Containing Semi-Markovian Switching Parameters," Proceedings of IEEE Conference on Decision and Control, 1971.

[4] R. L. Moose and D. H. McCabe, "An Extended Adaptive State Estimator for Maneuvering Target Tracking," IEEE Ninth Annual Southeastern Symposium on System Theory, Charlotte, N. C., 1977.